

國立臺灣大學生農學院生物產業機電工程學系

碩士論文

Department of Bio-Industrial Mechatronics Engineering

College of Bioresources and Agriculture

National Taiwan University

Master Thesis

基於物聯網之電力品質監測平台的開發

Development an IoT-Based Power Quality

Monitoring Platform

陳孟甫

Meng-Fu Chen

指導教授：周呈雲 博士

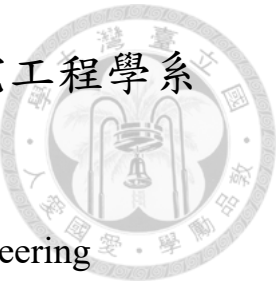
江昭皚 博士

Advisor: Cheng-Ying Chou, Ph.D.

Joe-Air Jiang, Ph.D.

中華民國 108 年 8 月

August 2019

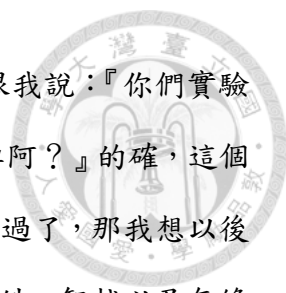




致謝

那個當初還在煩惱備取會不會上、沒考上的話要不要技術性延畢的準學士，在兩年後的今天，沒想到也成為了煩惱著致謝要怎麼寫的準碩士了。

決定讀碩士班的時候就對自己說過『如果兩年的時間可以學到很多東西，那再辛苦也要撐下去』。因此在確定備取上的時候就選擇了 303 與 105 的共同試驗，然而共同指導根本是一個我根本無法想像的煉獄級磨練。這兩年真的經歷了很多大學時期的我無法想像的事情，最稀鬆平常的大概是養成了超晚睡之後又超早起的習慣吧。能身心煎熬的順利度過這兩年，最感謝莫過於我微禿的好高大直屬奐絜、好大的前博士班學長楷勝以及好肥大的博士班學長育成中心的育誠。碩一的時候水源 303 的燈永遠過了半夜還亮著，裡面關著不停在加班的真夢幻地縛靈，而決定回家睡覺的契機大概就是有一個人喊：『欸！肚子好餓喔，要不要去吃永和豆漿』，之後其他兩個人就悻悻然得放下手邊的工作說著『明天再來加班好了...』。熬夜的碩一生活總是會有做不完的節點、除不完的 bug、寫不完的文件、每天吃的那家豆漿店以及轉角的全家便利商店，睡不飽的人生大概就像每天飄浮在空中。升碩二的暑假大概是我碩士生涯最爆炸的時候，那時候面臨節點組進度壓力、碩論進度壓力、研討會論文、要帶專題生與工讀生、幫忙實驗室的昆蟲工廠展示以及 105 的期中計畫報告，那個時候還以為要撐不下去了。很感謝奐絜那時幫忙帶了一陣子的學弟以及楷勝在展示時的 carry。另外也感謝秉良在我碩論剛起步的時候分擔了一段時間的節點組工作。寫碩論的時候，很感謝莎莎學長不停的跟我討論想法與實驗方向，常常丟一些有用的資料給我參考；感謝當兵中的奐絜時常打電話來關心我的進度與我討論該如何進行下一步；當然，楷勝是我論文中最軟的那一塊。另外也感謝，可嘉以及鈺芳在計畫結案時一起熬夜拼進度。



進入研究所後常常會跟朋友們分享實驗室的日常，很多朋友都跟我說：『你們實驗室這麼操，根本就像在工作一樣了吧！會不會有一天被操到掛掉阿？』的確，這個碩士班讀起來真的好累，但偶爾回頭想，如果這麼累的我都能熬過了，那我想以後再艱難的狀況都能撐過吧！謝謝碩士班的同學，侑倫、祥煜、聖皓、智越以及無緣的其諺與偉哲哥，很感謝大家一直以來很多的幫忙，也讓我在大家身上學習到很多。同時特別感謝我的指導教授 周呈雲教授，周老師是一位很關心學生生活狀況的老師，常常提醒我各種獎學金的申請以及系務事項的注意；也感謝我的共同指導教授 江昭皚教授與師母 王淑芬女士，江老師是一位樂於跟學生分擔研究上與計畫執行上壓力的老師，也很感謝師母時常對我們的關心，而收到江老師與師母送的畢業禮物，我真的很開心。當初備取上的時候有幸於兩位教授共同指導，在這兩年時常受到老師們的關懷與照顧，實在是學生之福，祝老師們與師母在將來能身體健康，計畫一年一年的過，論文一篇一篇的發。再者，感謝兩個實驗室的助理們與博後學長。感謝人正學長，雖然我很少找時間去跟學長討論論文，但學長始終沒有放棄我，耐心的跟我討論架構與論文的指導，我才能將論文順利完成；感謝瘦身有成的總管瑋哥在我面臨挫折的時候幫我做心靈上的開導，以及讓我買貴貴的東西；感謝慕華姊常常在期限前趕工指導我英文寫作的的能力；感謝珮怡及珊杉在總是幫忙處理許多採購與報帳的事物；感謝思廷在沒人管理實驗室的時候，幫忙建立實驗室規則與秩序，以及幫助我解決許多論文上與生活上的問題。

除了實驗室的同仁，也感謝我的大學同學大威與學弟證傑，以及中興生機系壘的肥宅們，很多壓力大的時候可以跟大家一起聊天講幹話，有空的時候一起出來嗨，吃難吃的老崔，希望未來在工作後的閒暇之餘也能約個時間一起回味老崔。也感謝高中同學家佑、冠億以及煒竣，每次回高雄都能約出來一起打球吃丹丹；感謝薇韻與諱莉，在我這個南部人初來台北時有個照應。

特別感謝我的家人，阿公、阿嬤、大伯、伯母、姑姑、姑丈還有哥哥姊姊們，如果今天能有什麼成就也是大家的功勞，是大家在我的人生中不斷的支持我前進，快撐不下去的時候給我鼓勵，讓我知道家是這麼的溫暖。

最後感謝的人是我自己，謝謝你沒有中途放棄，就算這麼辛苦你也是撐過了，一步一步的朝著你的目標邁進。謝謝你成為了那個能讓家人不再被看不起，提到你的名字的時候是充滿驕傲的說『這是我家的小孩』的人。希望在未來你能夠繼續努力成為有用的人，達成你對自己的期許，不讓愛你的人失望。繼續加油，後面是一個新的起點。

謹誌於

國立臺灣大學生物產業機電工程學系暨研究所

2019/08/19 2:40 P.M.



中文摘要



近年來，隨著高科技產業蓬勃發展，越來越多精密儀器被使用在生產線上，而這些儀器對於電力的敏感度也較高，稍微不良的電力品質即可能造成運作停止，使得供電環境要求比以往要來的嚴格許多。電力品質包含了電力系統中的電壓穩定度，輸出電流波形及頻率的正常性程度。而電力品質的優劣亦會影響到這些精密設備的耗電率及壽命，因此電力公司提供給用戶端的電力品質就顯得十分重要。有別於過去人們經常要攜帶大型感測儀器到設備現場才能對設備進行量測，以得到設備資訊。本論文提出一個主要針對短時間內的電壓變動以及異常波電壓事件進行辨識與偵測的即時電力品質監測系統，透過物聯網技術，架設可量測設備電力品質之感測節點，經由感測器量測電力設備輸出電壓及電流波形，再將量測訊號進行快速傅立葉分析以及離散小波轉換，與市售儀器之量測結果做一比較。另外，經由事件門檻值的設定，當量測設備偵測到不良之電力品質事件後，將透過閘道器將事件做初步分類，再將訊息轉傳至網路上再發出警報，以便做設備的維護及事件紀錄。

關鍵詞：電力品質、物聯網、快速傅立葉、離散小波轉換、設備品質

Abstract



In recent years, with the rapid development of high-tech industries, more and more precision instruments are used in the production line, and these instruments are also more sensitive to electricity. Slightly poor power quality may cause the operation to stop. Therefore, the environmental requirements for power supply are much stricter than ever. Power quality issues may include the stability of the voltage, and the normality of the output current waveform and frequency in the power system. The quality of power quality will also affect the power consumption and life of these precision equipment. Therefore, the power quality provided by a power company to the customer is very important. In the past, people often had to carry large-scale sensing instruments to the site to obtain the information of a power generation device, which was very inconvenient. This study therefore proposes a real-time power quality monitoring system that identifies and detects short-term voltage fluctuations and irregular harmonic voltage events. Using the Internet of Things technology, a sensing node capable of measuring the power quality is developed, and the output voltage and current waveform of the power generation device are measured by the sensor. The measuring signal is subjected to the Fast Fourier analysis and discrete wavelet transform. Finally, the analysis results are compared with the measurements of commercially available instruments. In addition, after the proposed sensor detects a bad

power quality event, the event will be classified by a gateway, and then the message will be transmitted to the network and then an alarm will be issued, so users can easily maintain power equipment and record the events.



Keywords—Power quality, Internet-of-Things, Fast Fourier transform, Discrete wavelet transform, Equipment quality

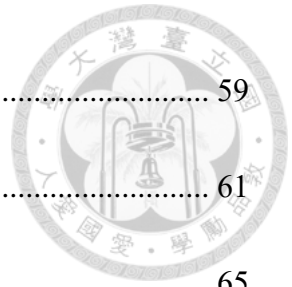
Table of Content



致謝	i
中文摘要	v
Abstract.....	vi
Table of Content	viii
List of Figures.....	xi
List of Tables	xv
Chapter 1 Introduction	1
1.1 Background.....	1
1.2 Motivation and Purpose.....	3
1.3 Structure of the Thesis	4
Chapter 2 Literature Review	7
2.1 Introduction of Power Quality	7
2.2 Event Types of Power Quality	8
2.2.1 Voltage Swell	10
2.2.2 Voltage Sag	11
2.2.3 Voltage Interruption	12
2.2.4 Harmonic	13

2.3	Different Power Quality Monitoring Methods	18
2.3.2	An Internet -Based Power Quality Monitoring System.....	21
2.3.3	Dual Core Sensing System	22
2.3.4	Power Quality Monitoring over Smartphones.....	24
2.3.5	A Smart Meter Composed of FPGA and Bluetooth	25
2.4	Algorithms for Analyzing Power Quality Events.....	27
Chapter 3	Method.....	31
3.1	Poor Power Quality Event Detection	31
3.1.1	Irregular Voltage Events	32
3.1.2	Irregular Harmonic Event.....	34
3.2	Fast Fourier Transform	34
3.2.1	DIT of FFT	36
3.2.2	DIF of FFT	38
3.2.3	Limitations and Effects of FFT	40
3.3	Wavelet Transform	42
3.4	Power Quality Monitoring System.....	48
3.5	Network Time Protocol (NTP)	58
Chapter 4	Results and Discussion	59

4.1	Relay Testing System	59
4.2	System Verification.....	61
4.3	Verify the System with Poor Power Quality Events.....	65
4.3.1	Voltage Swell	65
4.3.2	Voltage Sag	68
4.3.3	Voltage Interruption	71
4.3.4	Harmonics.....	74
4.3.5	Spectrogram of Poor Power Quality Event	79
4.4	Field Experiment	84
4.4.1	Transmission and Receiving Rate of Wireless Transmission.....	84
4.4.2	Power Quality Event Classification.....	86
Chapter 5	Conclusions and Future work	93
References	95



List of Figures

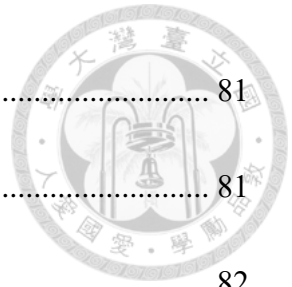


Figure 1-1	Two aspects of power quality	2
Figure 1-2	Information regarding the power sag accident in Taiwan	2
Figure 2-1	Causes for poor power quality	8
Figure 2-2	Waveforms of a voltage swell.....	11
Figure 2-3	Waveforms of a voltage sag.....	12
Figure 2-4	Waveform of the voltage interruption.....	13
Figure 2-5	An Internet -Based Power Quality Monitoring System.....	22
Figure 2-6	Block diagram for the power quality monitoring device.....	23
Figure 2-7	Power quality monitoring over smartphones.....	25
Figure 2-8	Functional diagram for the smart meter	26
Figure 2-9	Developed smart meter and its internal components.....	27
Figure 3-1	The flow chart of the determination of an irregular voltage.....	33
Figure 3-2	The flow chart of determining an irregular harmonic	34
Figure 3-3	Simple 8-point DIT of FFT	38
Figure 3-4	Simple 8-point DIF of FFT.....	40
Figure 3-5	Fixed window size of the STFT	43
Figure 3-6	Window size of a wavelet.....	44

Figure 3-7	The decomposition diagram of the first order wavelet transform	46
Figure 3-8	The composition diagram of the first order wavelet transform	46
Figure 3-9	Discrete signal as layer α in the discrete wavelet transform architecture	47
Figure 3-10	Appearance of the IoT-based PQ sensor.....	49
Figure 3-11	System flowchart	49
Figure 3-12	System architecture.....	50
Figure 3-13	Appearance of the CT.....	53
Figure 3-14	Comparison of different wireless transmission protocols.	54
Figure 3-15	Comparison of the power consumption for each transmission protocol. ...	55
Figure 3-16	ZigBee wireless transmission module	55
Figure 3-17	Principle of the sensing circuit	56
Figure 3-18	Circuit diagram of PQ sensor	57
Figure 4-1	OMICRON CMC 356	61
Figure 4-2	Different sampling frequencies of the PQ sensor	62
Figure 4-3	Sampling results of different instruments under ideal waveform.....	64
Figure 4-4	Comparison of ideal waveforms after FFT.....	64
Figure 4-5	Sampling results of different instruments under voltage swell	66
Figure 4-6	Comparison of voltage swell after FFT	67

Figure 4-7 DWT results of the voltage swell via the recorder	67
Figure 4-8 DWT results of the voltage swell via the PQ sensor	68
Figure 4-9 Sampling results of different instruments under voltage sag	69
Figure 4-10 Comparison of voltage sag after FFT	70
Figure 4-11 DWT results of the voltage swell via the recorder	70
Figure 4-12 DWT results of the voltage sag via the PQ sensor	71
Figure 4-13 Sampling results of different instruments under voltage interruption	72
Figure 4-14 Comparison of voltage interruption after FFT	72
Figure 4-15 DWT results of the voltage interruption via the recorder	73
Figure 4-16 DWT results of the voltage interruption via the PQ sensor	73
Figure 4-17 Case 1 measured by two devices	74
Figure 4-18 Comparison of case 1 after FFT	75
Figure 4-19 Case 2 measured by two devices	76
Figure 4-20 Comparison of case 2 after FFT	76
Figure 4-21 Case 3 measured by two devices	77
Figure 4-22 Comparison of case 3 after FFT	78
Figure 4-23 Current harmonics measured by two devices	79
Figure 4-24 The spectrogram of voltage swell event	80

Figure 4-25 The spectrogram of voltage sag event	81
Figure 4-26 The spectrogram of voltage interruption event.....	81
Figure 4-27 The spectrogram of harmonic case 1	82
Figure 4-28 The spectrogram of harmonic case 2	83
Figure 4-29 The spectrogram of harmonic case 3	83
Figure 4-30 System equipment location map.....	85
Figure 4-31 Transmission and receiving rate from different room	86



List of Tables



Table 2-1	Event types of power quality.	9
Table 2-2	Degree of harmonic interference of electronic equipment.	16
Table 2-3	Harmonic voltage limits established by IEEE.	17
Table 2-4	Harmonic current limits established by IEEE.	18
Table 2-5	Comparison of different power quality monitoring methods.	19
Table 2-6	Advantages and disadvantages of employing different power quality monitoring methods.	20
Table 3-1	Specifications of the MCU.	51
Table 3-2	Specifications of the CT	52
Table 4-1	Operational script for one power quality events.....	88
Table 4-2	Accuracy of one event classification.	89
Table 4-3	THD of unsuccessful classification events.....	90
Table 4-4	Operational script for two power quality events.	91
Table 4-5	Accuracy of tow event classification.....	92



Chapter 1 Introduction

1.1 Background

Electrical equipment is closely related to people's lives and so does the electricity. With the rapid development of high-tech and commercial industries, more electronic products are used for loads, computer equipment and precision instruments. Poor power quality (Cristaldi and Ferrero, 1995; Gray and Haydock, 1995; Kazibwe, *et al.*, 1990; Lentz, *et al.*, 1995; Reid, 1996) may cause these instruments to operate abnormally or malfunction, or even cause equipment damage, which will affect the production schedules and eventually bring economic losses. For example, harmonics will cause the reactor to burn out or the capacitor to make an irregular sound. Pulse noise or voltage drops also cause the control system to stop. The abnormality of power lines due to the deterioration of the power quality is a problem common to both the power supply side and the user side. However, in reality, it is very difficult to determine the direct cause of the power system anomaly. In order to identify the direct cause, it is necessary to perform power quality measurement in order to implement an effective countermeasure. Power quality problems usually have two points to judge (Bollen, 2000), one is power supply reliability, and the other is voltage quality. The power quality interference of a general power system

can be judged from the variation of four parameters such as frequency, size, waveform, and symmetry. If the power equipment receives power of poor quality for a long time, the equipment is damaged, resulting in a large-scale power outage.

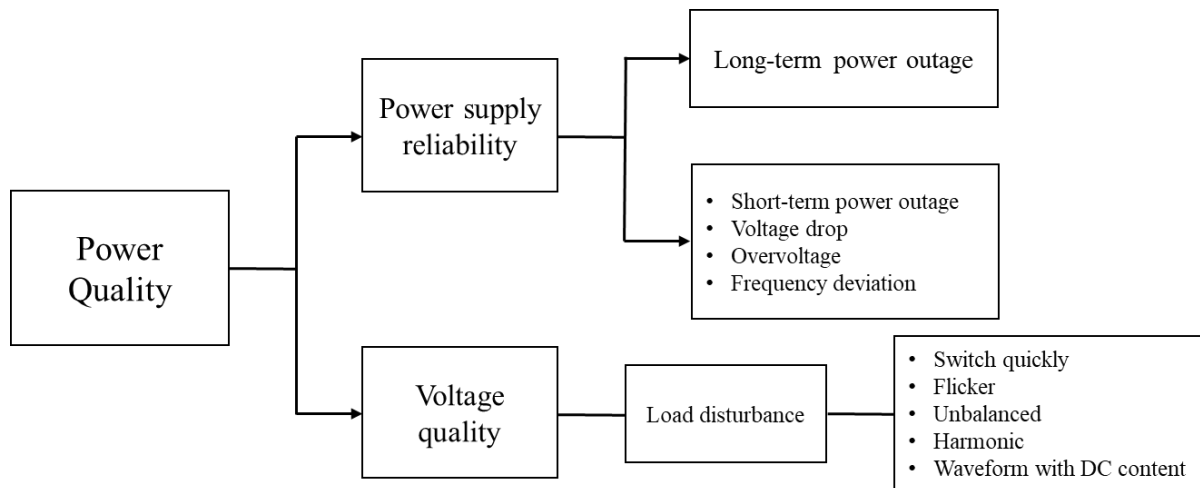


Figure 1-1 Two aspects of power quality.

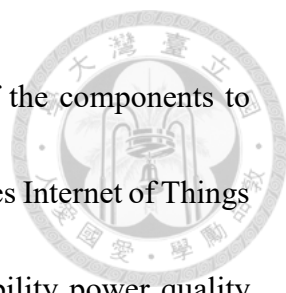


Figure 1-2 Information regarding the power sag accident in Taiwan.

As shown in Figure 1-2 above, in 2018, due to the failure of 161KV UHV large user equipment in Taoyuan, the voltage of the adjacent transmission system suddenly dropped, which not only caused a short suspension of power in North Taiwan, but also caused the production line of surrounding technology plants to stagnate, bringing more than 200 million economic losses.

1.2 Motivation and Purpose

There are many power quality monitoring instruments manufactured by different companies on the market. However, most of these commercially available power quality analyzers must rely on on-site personnel to operate, and only the personnel in the area are responsible for management. It is difficult to monitor and control various types of power equipment scattered around the power plant. Therefore, a system that integrates information about the power equipment in various areas has become an important issue for a power system, and such a system is also one of the most important developments for modern smart grids. The power company needs to know the operation of each piece of the equipment to determine the quality of the equipment. The precautionary maintenance must be carried out before the equipment is seriously damaged. A complete equipment information system must include the information regarding real-time equipment status, the record of bad power quality events and types, master the current



use of the equipment, and repair logs that show the replacement of the components to avoid serious damage. Therefore, this study proposes a system that uses Internet of Things technology to design a low-cost, high-precision, and high-compatibility power quality test platform. The output current and voltage waveform of the power equipment can be directly measured, and the monitoring personnel can complete the simple settings. It is not necessary for inspectors to go to the site in person to deal with a bad power quality event in the area. Through the network, the function of controlling the condition of the equipment in time can be effectively achieved.

1.3 Structure of the Thesis

This thesis develops a power quality monitoring system based on Internet of Things technology. It includes five chapters. The first chapter explains the research background, research motivation, thesis structure and the contribution of the thesis. The second chapter provides an overview of power quality, the types of power quality events, and methods used to monitor power quality in the past. It concludes with a summary. The third chapter first describes the power quality event simulator used in the study. Then, the power quality monitoring system proposed by the study is introduced, including the hardware design and the presentation of a visual interface. Finally, the technology used for analyzing the waveform data is discussed. The fourth chapter explains the experimental results. The

experiment measures the voltage and current waveforms of power equipment and evaluates power quality events under a normal operation. The commercially available instruments are used as the standard to examine the performance of the proposed monitoring system. After analyzed by different waveform techniques, the monitoring performance of the standard instruments and the proposed monitoring system is compared, including measurement accuracy and applicability. Finally, the fifth chapter summarizes the research results and explains future research directions.





Chapter 2 Literature Review



Chapter 2 lists some information and literature about power quality, event types of power quality and the effects of these events. In addition, methods used to monitor the power quality and analyze a voltage event are also discussed in this chapter.

2.1 Introduction of Power Quality

The power quality specification is a measure of the quality of a voltage, current waveform, and frequency in a power system. The power normally sent by the power plant is a standard sinusoidal waveform, and the cause of poor power quality may be transient voltage changes caused by accidents, such as bad weather, equipment failure, human factors and animal factors. In addition, harmonic pollution caused by non-linear load equipment in the power system, and voltage flicker caused by large-scale vibration caused by construction also affect power quality.

Regarding the definition of power quality, the Institute of Electrical and Electronics Engineers (IEEE) and the Canadian Electric Association (CEA) put forward different views. The former defines power in the position of the power company. For this viewpoint, the quality is the acceptance of the power system to the pollution source. The latter is based on the user's position, defining the power quality as the user's satisfaction with the power supply quality of the power company (Jiang, 2007). It can be seen that the power

quality must be accepted by both power providers and power users, and the basis for their definition must be regulated by power quality control standards.

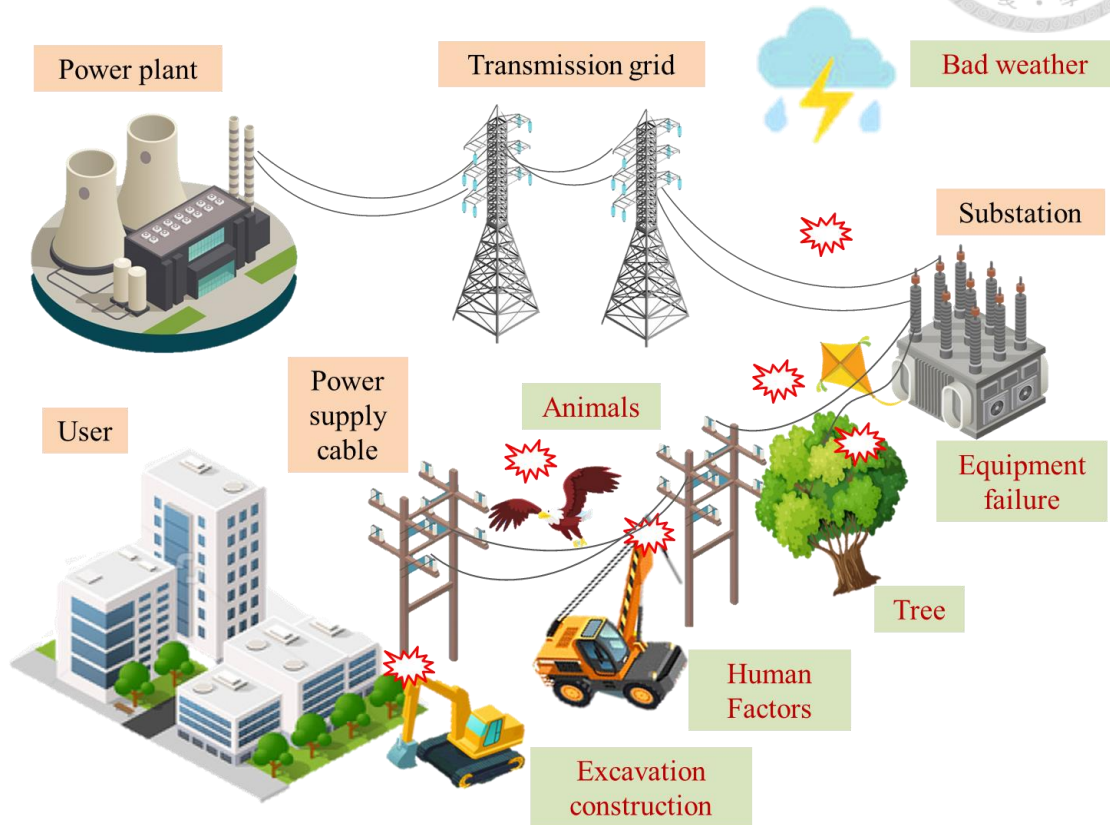


Figure 2-1 Causes for poor power quality.

2.2 Event Types of Power Quality

The IEEE power quality monitoring standard, IEEE Std. 1159-2009 ("IEEE Std 1159-2009 ", 2009), published in 2009, provides a detailed introduction to power quality event types. The phenomenon of power system interference can be divided into transient changes, short-term changes, long-term changes, three-phase unbalance, waveform distortion, voltage flicker, power frequency fluctuations and other events.

Table 2-1 Event types of power quality ("IEEE Std 1159-2009", 2009).

Types of event			Frequency domain distribution	Duration	Voltage range
Transient	Impulsive	Nanosecond	Rising time 5 ns	< 50 ns	
		Microsecond	Rising time 1 μ s	50ns - 1 ms	
		Millisecond	Rising time 0.1 ms	> 1 ms	
	Oscillatory	Nanosecond	< 5 kHz	0.3 - 50 ms	0 - 4 pu
		Microsecond	5 - 500 kHz	20 μ s	0 - 8 pu
		Millisecond	0.5 - 5 MHz	5 μ s	0 - 4 pu
Short duration variation	Instantaneous	Interruption		0.5-30 cycles	< 0.1pu
		Sag		0.5-31 cycles	0.1 - 0.9 pu
		Swell		0.5-32 cycles	1.1 - 1.8 pu
	Momentary	Interruption		30 cycles-3 s	< 0.1 pu
		Sag		31 cycles-3 s	0.1 - 0.9 pu
		Swell		32 cycles-3 s	1.1 - 1.4 pu
	Temporary	Interruption		3 s - 1 min	< 0.1 pu
		Sag		3 s - 2 min	0.1 - 0.9 pu
		Swell		3 s - 3 min	1.1 - 1.2 pu
Long duration variation	Sustained Interruption			> 1 min	0 pu
	Undervoltage			> 2 min	0.8 - 0.9 pu
	Overvoltage			> 3 min	1.1 - 1.2 pu
Voltage imbalance				Steady state	0.5 - 2 %
Waveform distortion	DC offset	0 - 9 kHz		Steady state	
	Harmonics	0 - 10 kHz		Steady state	
	Interharmonics	0 - 11 kHz		Steady state	
	Notching			Steady state	
	Noise	Broadband		Steady state	
Voltage flicker		< 25 kHz		Intermittent	
Power frequency change				< 10 s	\pm 0.1 Hz




Table 2.1 lists the classification and definition of power system interference phenomena mentioned in IEEE Std. 1159-2009. Therefore, power providers and power users can measure the quality of power according to this specification. As can be seen in Table 2.1, there are many types of power quality events. However, this study only identifies and analyzes transient voltage fluctuations and harmonic interference. The following describes the types of events for voltage fluctuations.

2.2.1 Voltage Swell

A voltage swell is defined as an increase in the RMS voltage or current at the supply frequency, with a duration of 0.5 cycles to 1 minute. Typical amplitudes range from 1.1 pu to 1.8 pu. The magnitude of the swell is also described by its remaining voltage, which in this case is always greater than 1.0 pu (Naidoo and Pillay, 2007), as shown in Figure 2-2, the voltage swell may be caused by transient phenomena caused by single-phase ground faults, large-capacity motor stops, sudden load drops, large-capacity capacitor banks, and lightning strikes. The voltage swell can cause damage to electrical equipment and shorten the life of the equipment.

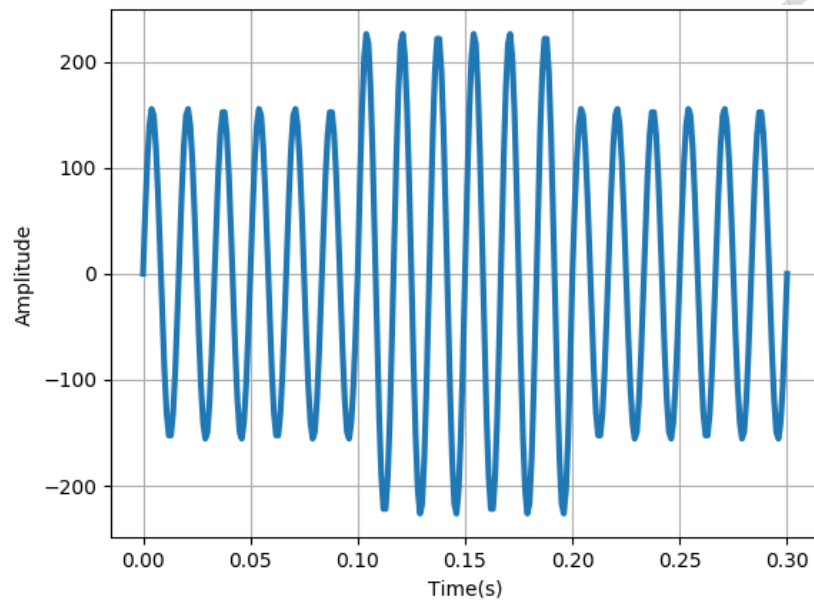


Figure 2-2 Waveforms of a voltage swell.

2.2.2 Voltage Sag

A voltage sag is defined as the drop in the root mean square (RMS) voltage at the supply frequency, with a duration of 0.5 cycles to 1 minute (Bollen, 2000). The duration of the voltage dip is the measurement time when the RMS value of voltage drops below the nominal voltage of 0.9 pu and rises above the nominal voltage of 0.9 pu, as shown in Figure 2-3. The voltage sag does not represent a power outage, and the power supply is uninterrupted during the occurrence. This may be caused by the flow of the inrush current or fault current associated with the start of the motor load due to the temporary disconnection of the power-related switching operation. These events may come from customer systems or from public supply networks. Therefore, a short sag may cause

problems to some sensitive devices. For example, it may cause a control device to malfunction, a computer to shut down, and a motor to change its speed or stop.

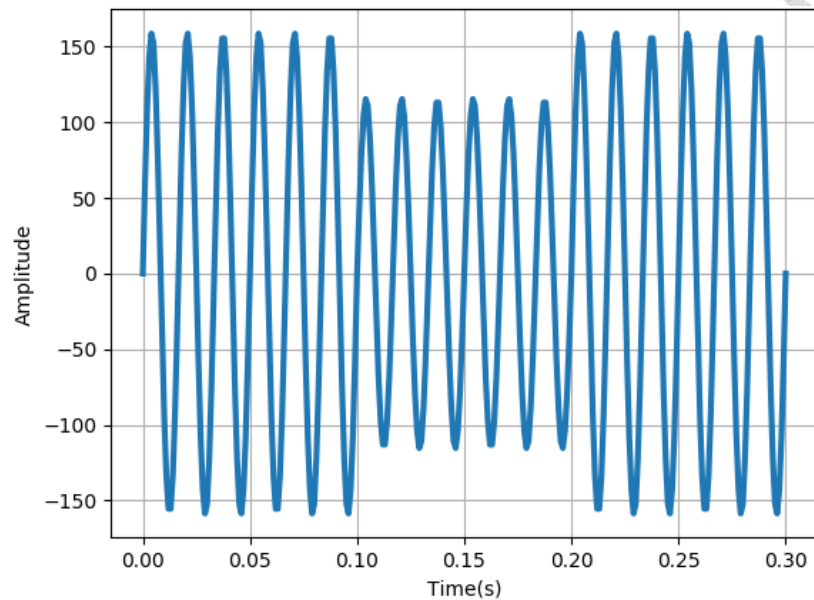


Figure 2-3 Waveforms of a voltage sag.

2.2.3 Voltage Interruption

The voltage interruption means that the voltage drops below 0.1 pu on the power line for 0.5 to 1 minute, as shown in Figure 2-4, if the power is interrupted for more than one minute, a permanent failure that cannot be eliminated by the switch may occur. At this time, it is necessary to rely on human intervention to eliminate the failure and restore the power supply. The cause of the voltage interruption may be due to a system short-circuit fault that causes the power fuse to blow or the circuit breaker to trip, the power equipment to malfunction, and the control failure.

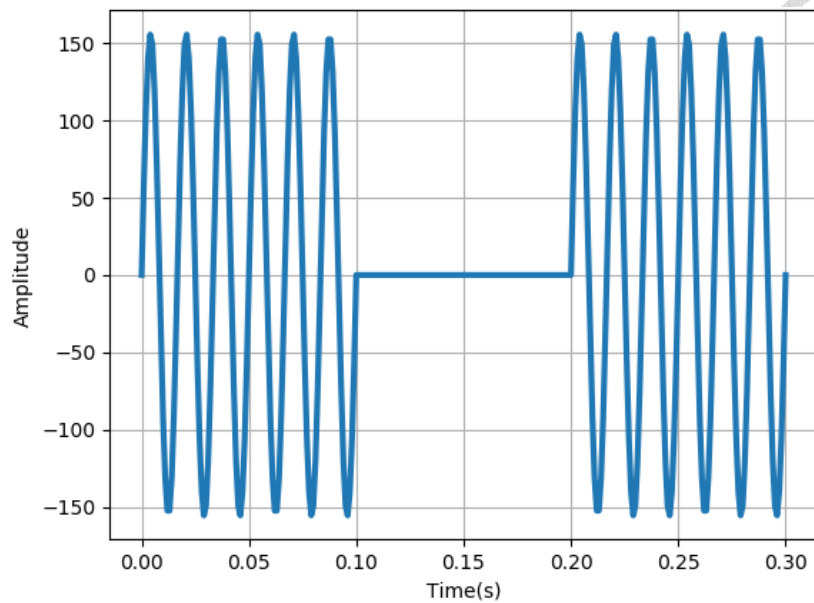


Figure 2-4 Waveform of the voltage interruption.

2.2.4 Harmonic

In a power system, when a sinusoidal wave is applied to a non-linear load, the current of the non-linear load itself is not proportional to the supplied voltage, resulting in a periodic distortion current. When the harmonic current passes through the impedance of the system, it leads to the generation of harmonic voltage (Liu *et al.*, 2005). The typical nonlinear load types are as follows:

(a) Iron core excitation: synchronous generators, transformers, etc.;

(b) Arc load: electric arc furnace, arc welding machine, etc.;

and (c) Power electronic circuits: this type is the main harmonic source in the power system, such as rectifiers, inverters, personal computers and home appliances.

According to the theory proposed by Joseph Fourier in 1822, any continuous periodic function can be expressed as a linear combination of a fundamental wave and a sine wave component of an integer multiple of the fundamental wave frequency. The sum of these sinusoidal functions is called the Fourier series. The concept of Fourier series is often used to analyze harmonic problems (Bonner, *et al.*, 1996). Usually expressed in terms of individual harmonic distortion factor and total harmonic distortion factor.

$$f(t) = A_0 + \sum_{n=1}^{\infty} A_n \cos(n\omega_0 t + \theta_n) \quad (2-1)$$

where ω_0 is the base frequency, and A_0 is the DC component of the function, is defined as:

$$A_0 = \frac{1}{T} \int_0^T f(t) dt \quad (2-2)$$

where $T = \frac{2\pi}{\omega_0}$

A_n and θ_n are the coefficients of the n^{th} harmonic and the phase angle, which can be expressed as

$$A_n = \sqrt{B_n^2 + C_n^2} \quad (2-3)$$

$$\theta_n = \tan^{-1} \frac{B_n}{C_n} \quad (2-4)$$

Also, B_n and C_n are defined as

$$B_n = \frac{2}{T} \int_0^T f(t) \cos(n\omega_0 t) dt \quad (2-5)$$

$$C_n = \frac{2}{T} \int_0^T f(t) \sin(n\omega_0 t) dt \quad (2-6)$$

where $T = \frac{2\pi}{\omega_0}$

The root mean square value (RMS) of the periodic function $f(t)$ is defined as



$$RMS = \sqrt{A_0^2 + \sum_{n=1}^{\infty} (A_n^2 / \sqrt{2})^2} \quad (2-7)$$

In order to express the degree of harmonic distortion, the Total Harmonic Distortion (THD) and the Total Demand Distortion (TDD) are often used as indicators. Since V_1 and I_1 is the fundamental frequency voltage and current, n starts from 2. Also, V_n and I_n are the n^{th} harmonic voltage and current. The formula for the Total Voltage Harmonic Distortion Factor (THD_V) and the Total Demand Distortion (TDD) is as follows:

$$THD_V = \frac{\sqrt{\sum_{n=2}^{\infty} V_n^2}}{V_1} = \frac{\sqrt{V_2^2 + V_3^2 + V_4^2 + \dots + V_n^2}}{V_1} \quad (2-8)$$

$$TDD_I = \frac{\sqrt{\sum_{n=2}^{\infty} I_n^2}}{I_1} = \frac{\sqrt{I_2^2 + I_3^2 + I_4^2 + \dots + I_n^2}}{I_1} \quad (2-9)$$

When the harmonic content is too large, the transformer may be overheated, overloaded or even burned, the motor may generate noise, the capacitor may be destroyed due to

harmonic resonance, the fuse may be burnt out, or the power supply may be malfunctioned.

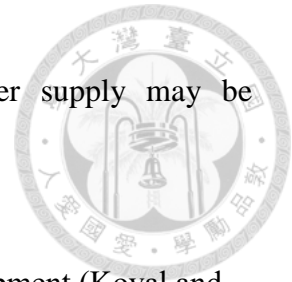


Table 2-2 Degree of harmonic interference of electronic equipment (Koval and Carter, 1997) .

Level of obstacle	Influence on the instrument	Situation	Result	Reason
Level 0	No effect	Functional characteristics do not change	N/A	N/A
Level 1	Minor failure	Allows for temporary loss of functionality, but not enough to fail	Shorter life, lower reliability, performance degradation	Due to excessive temperature rise, the failure rate rises temporarily and cannot function properly.
Level 2	Serious failure	Temporary action or characteristic failure that can be automatically recovered	Loss of function	Only temporarily lost functionality and can be automatically restored
Level 3	Fault criticality	Action or feature damage, must be manually restarted	Protection circuit action	Protection circuit action causes the machine to stop working
Level 4	Damage	Loss of function, equipment damage cannot be restored	N/A	N/A

Therefore, the Institute of Electrical and Electronics Engineers (IEEE) has established a set of harmonic control standards called IEEE Std. 519-1992 ("IEEE Std 519-1992," 1993). The content is widely used by the industry and power companies to control harmonic voltage and harmonic current. Table 2.3 and Table 2.4 list the limits of harmonic voltage and harmonic current.

Table 2-3 Harmonic voltage limits established by IEEE ("IEEE Std 519-1992," 1993).

Voltage of PCC bus	Individual distortion rate of harmonic voltage (%)	Total distortion rate of harmonic voltage (%)
Below 69 kV (inclusive)	3.0	5.0
69,001 V-161 KV	1.5	2.5
Above 161,001 V	1.0	1.5
Note:	(a) PCC: Point of Common Coupling (b) For short-time start-up and non-recurring harmonics, the above table limit can exceed 50 %.	

Table 2-4 Harmonic current limits established by IEEE ("IEEE Std 519-1992," 1993).

Harmonic distortion rate of current (%)						
Individual harmonic values at each level (odd)						
I_{sc}/I_L	$n < 11$	$11 \leq n < 17$	$17 \leq n < 23$	$23 \leq n < 35$	$35 < n$	TDD
< 20	4	2.0	1.5	0.6	0.3	5.0
20 ~ 50	7	3.5	2.5	1.0	0.5	8.0
50 ~ 100	10	4.5	4.0	1.5	0.7	12.0
100 ~ 1000	12	5.5	5.0	2.0	1.0	15.0
> 1000	15	7.0	6.0	2.5	1.4	20.0
Note:	* All power generation equipment is limited by $I_{sc} / I_L < 20$.					
	(a) The even harmonic limit value is 25 % of the odd harmonic limit value listed above.					
	(b) 69,001 – 161,000 V system is 50 % of the above limit.					
	I_{sc} : The maximum short-circuit current at the common coupling point (PCC). I_L : Maximum load current at PCC (fundamental frequency component).					

2.3 Different Power Quality Monitoring Methods

Many scholars have studied the issue of power quality, and it is very important to detect which power quality event is used in the initial stage of the system design. A number of monitoring methods have been proposed according to the selection of hardware and the algorithm used to analyze the power quality.

Table 2-5 Comparison of different power quality monitoring methods.

	Error	Feasibility in Wide Field Implementation	Probability of being used in real-time monitoring
Power quality analyzer	0.01 %	Bad	No
Zhang and Li	N/A	Good	Yes
Song <i>et al.</i>	0.12 %	Good	Yes
Huang <i>et al.</i>	0.1 %	Bad	Yes
Morales-Velazquez <i>et al.</i>	N/A	Bad	No

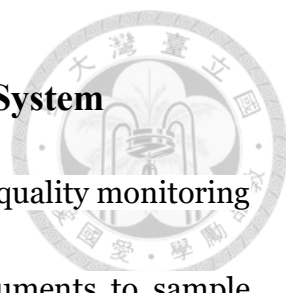
Table 2-5 shows the comparison of all methods for power quality measurement mentioned in this chapter. The approaches allowed the client and the PQN instrument to transmit data through an Ethernet network, so it was bound to receive terrain restrictions due to the wired transmission. And the system with two high-end processors, DSP and CPLD, the high price of these two processors made the system difficult to be widely used. For the method used smart phones as signal processors, which required high energy to operate. If there was no external power supply, it would be a challenge for the method to be widely used in the microgrid. Finally, a smart sensor based on FPGA technology in 2017. Because FPGA was difficult to be developed in software, and high power

consumption is also one of its shortcomings, the method could not be used for a long time without power supply. In addition, as a wireless transmission module, Bluetooth would not be able to provide sufficient transmission distance. A general description on the power quality literature will be given in the following subsections.

Table 2-6 Advantages and disadvantages of employing different power quality monitoring methods.

	Advantages	Disadvantages
Power quality analyzer	High measurement accuracy	High price Field use Manual classification failure
Zhang and Li	Unified management of data	Terrain restrictions due to the wired transmission
Song <i>et al.</i>	High accuracy	Not easy to use widely due to high price
Huang <i>et al.</i>	Low cost High accuracy	High power consumption, difficult to use widely
Morales-Velazquez <i>et al.</i>	Wireless transmission of sensing data	Energy consumption and small transmission distance

2.3.2 An Internet -Based Power Quality Monitoring System



In 2009, Zhang and Li (2009) proposed a system for power quality monitoring over the Internet. They mentioned that they used PQM instruments to sample voltage and current waveforms. Then provide the data to the site data manager client software. All PQMs are connected to the local network and use a unique GPS-based time synchronization. In this way, all information from different locations can be monitored on the same chart and on the same time base. The site client software implements industry-standard power monitoring data management for collecting, storing, and compressing power quality data generated by PQM. The network connects the client and server through the TCP/IP protocol. The onboard web server is combined with an Ethernet port to provide fast and easy access to real-time energy and basic power quality information without special software. Since the PQM holds all the data from each phase (current and voltage) with a resolution of up to 1024 samples per cycle, there is no need to speculate where the event occurred and how to create a set point to capture the event when the next event occurs. When the event first occurs, it is recorded by the PQM. Engineers only need to call the date and time of the event from various PQMs and view them on the same timeline using

Investigator client software, then use the investigator client software to compress and store the raw data for future analysis.

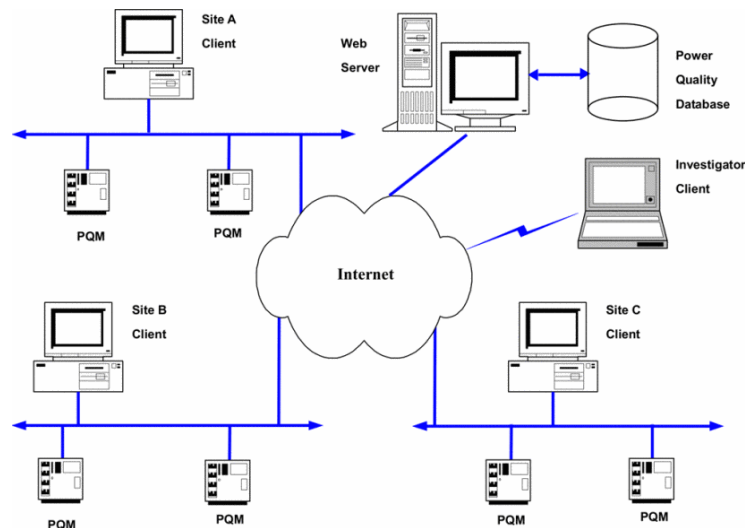


Figure 2-5 An Internet -Based Power Quality Monitoring System (Zhang and Li, 2009).

2.3.3 Dual Core Sensing System

In 2011, Song *et al.* (2011) proposed a power quality monitoring system based on Digital Signal Processor (DSP) and complex programmable logic device (CPLD). The power parameters were calculated by DSP and measured by CPLD. The main idea of the electrical parameter detection system is to use TMS320F2812 to form a digital processing system. The lower-level computer is mainly used for real-time sampling, data processing, analysis and short-term storage, and then communicates with the upper-layer data communication computer. The DSP is a wafer that is made to meet specific needs, so the

steps of building hardware can be eliminated. Due to the limitations of hardware, DSP enhances data processing and computing capabilities, allowing users to focus on the development of algorithms. In this paper, DSP completes software filtering, FFT calculation, calculation, detection, and various judgments of voltage parameters, such as voltage, current, power, harmonics, etc., required data storage. If the data exceeds the limit, the DSP controls the corresponding output relay and sends an alarm message from the external power system. Using the watchdog to perform refresh, reset and real-time detection systems. Although this system is equipped with two high-end processors, DSP and CPLD, however, the high price of these two processors makes it difficult to be widely used.

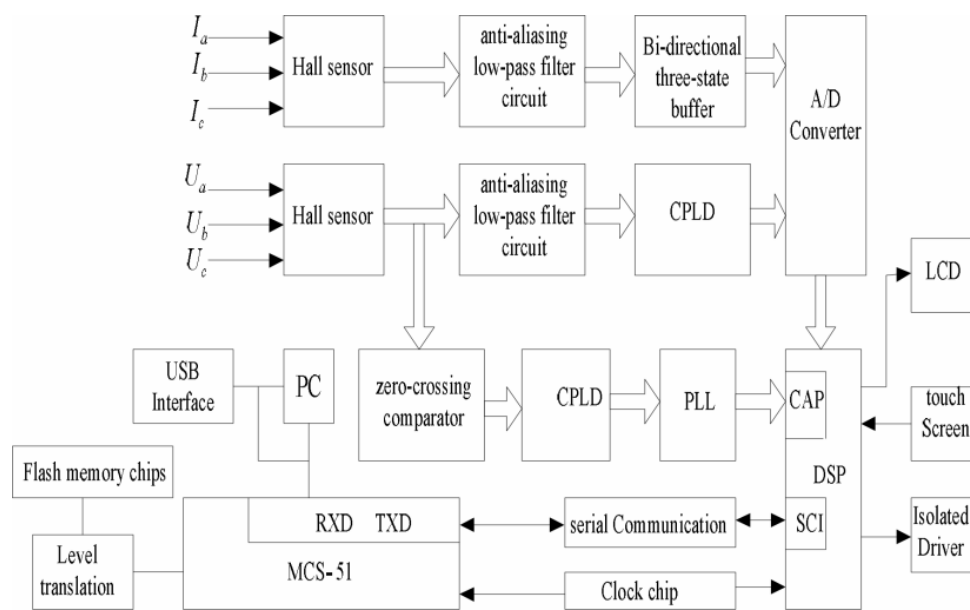
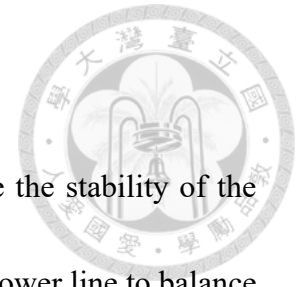


Figure 2-6 Block diagram for the power quality monitoring device (Song, *et al.*,

2011).

2.3.4 Power Quality Monitoring over Smartphones



In 2016, Huang *et al.* (2016) believed that in order to achieve the stability of the microgrid, it is necessary to monitor the power quality through the power line to balance demand and power generation. However, unreliable data collection makes control very difficult and the existing method (PMU) is very expensive. Therefore, a detailed design of a low-cost home sensing hardware is proposed. The main challenge of sensing hardware is time synchronization between sensors. Since self-sustainable microgrids need to monitor energy data from all households in real time, it is necessary to accurately synchronize readings from different households. The sensing hardware includes a voltage regulator module, a voltage conversion circuit, a microprocessor-based analog-to-digital (AD) sampling module, a PSS acquisition circuit, and an Android-based smartphone. The voltage regulator outputs the necessary DC power to power the entire system, including the smartphone. The voltage conversion circuit takes an analog voltage signal from a 120 V wall outlet and converts the AC power to a voltage range for analog-to-digital conversion (ADC). An 8-bit microprocessor (MCU) is used to control the voltage sampling process at an external ADC with a sampling frequency of 1440 Hz and send the data to the smartphone every 100 ms for phasor state estimation. Because this system uses smart phones as signal processors, and the required energy consumption is quite large, if

there is no external power supply, it seems to be a challenge to use it widely in the microgrid.

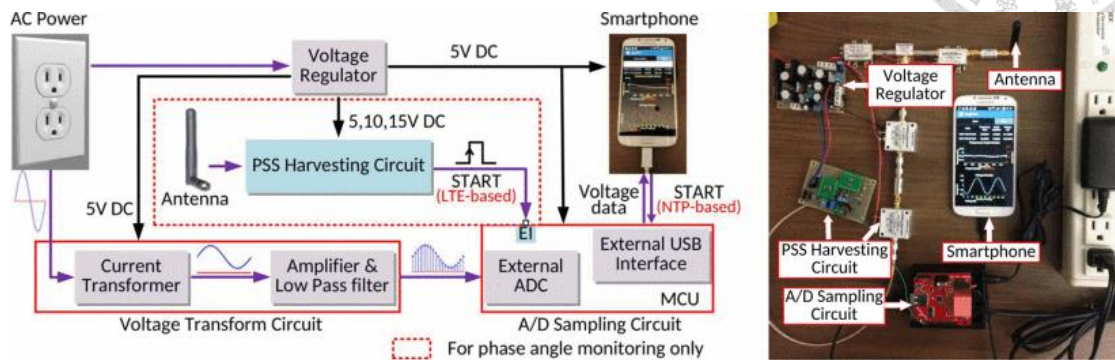


Figure 2-7 Power quality monitoring over smartphones (Huang, *et al.*, 2016).

2.3.5 A Smart Meter Composed of FPGA and Bluetooth

In 2017, Luis Morales-Velazquez *et al.* proposed a smart sensor-based intelligent sensor network based on FPGA technology; it integrates data acquisition modules, storage devices and wireless Bluetooth communication modules. The advantage is that the required hardware functions can be designed and parallel processed, and can handle communication between multiple modules at the same time, but the software development is more difficult, so the general internal logic components of the FPGA are used to synthesize Nios. II processor. High-end data processing and computing with this processor. To integrate intelligent sensor networks, the system utilizes mobile devices such as smartphones or tablets that synchronize smart sensors and remotely monitor them. The smart sensor is based on the Xilinx® FPGASpartan6 (XC6SLX16) and 16-bit

analog-to-digital converter with eight Texas Instruments (ADS130E08) channels providing up to 8000 samples per second. The voltage signal is obtained by the resistance divisor between each phase and the neutral point; at the same time, the current is obtained from the commercial current: Fluke®i200, Fluke®i400 and Fluke®i3000s-FLEX. Both voltage and current are isolated from the measurement system by an isolation amplifier. The proposed smart sensor is located in a non-intrusive device because there is no need to suspend energy flow during installation, unloading and operation.

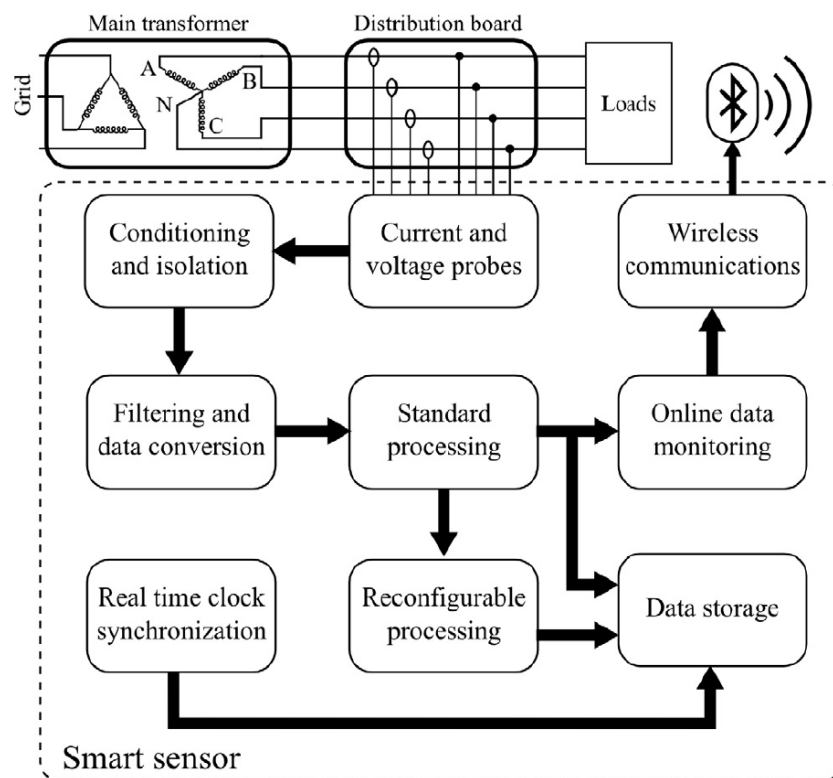


Figure 2-8 Functional diagram for the smart meter (Morales-Velazquez, *et al.*,

2017).

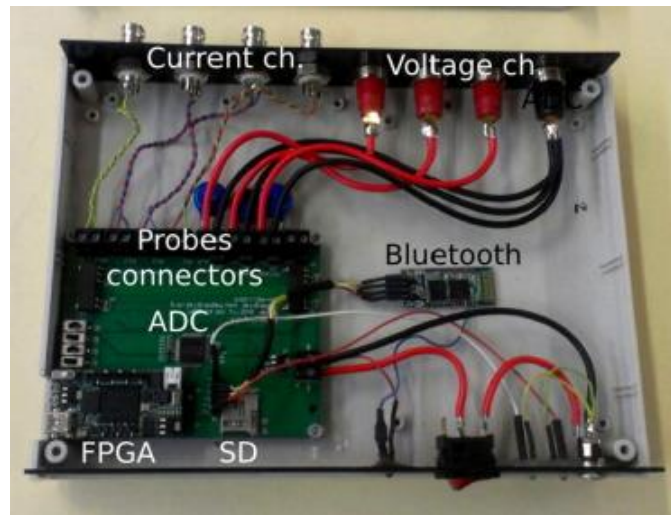
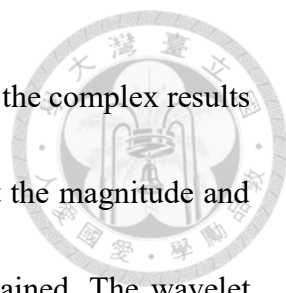


Figure 2-9 Developed smart meter and its internal components (Morales-Velazquez, *et al.*, 2017).

2.4 Algorithms for Analyzing Power Quality Events

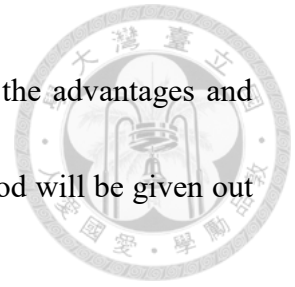
In the algorithm of power quality event analysis, the most intuitive method is to design algorithms based on the characteristics of the original waveform in the time domain, such as: Zero-Crossing method (Begovic, *et al.*, 1993; Chen and Lan, 2014; Mog and Ribeiro, 2004). The operation speed in the time domain is fast, and the analysis can be directly performed on the discrete signals, but it may be affected by the signal frequency, noise interference or DC bias, which causes errors in the calculation results. And there is another method to perform analysis in the frequency domain, usually by Fourier transform and wavelet transform, to detect signal characteristics that cannot be observed in the time domain. In the literature (Dash, *et al.*, 2003; Jurado and Saenz, 2002), the short-time Fourier transform (STFT) has been used. In the case of discrete time, the



data is cut into a number of large frames. The STFT method is to add the complex results obtained after each group of frames to the Fourier transform, so that the magnitude and phase of the time and frequency changes of each point can be obtained. The wavelet transform not only can flexibly design the accuracy of the frequency domain and of the time domain but also analyze the original signal at multiple levels, as pointed out in (Lang, *et al.*, 1996), the wavelet transform can effectively eliminate transient noise to improve the detection accuracy.

Based on the above review and comparison, the goal of this study is to establish an accurate, feasible, and stable system to directly measure the time domain waveforms of voltage and current and provide them in real time to achieve power quality monitoring. The real-time data transmission from the device to the database through wireless communication technology achieves the purpose of real-time measurement and monitoring. In addition, in order to verify the reliability of the monitoring system, this paper uses fast Fourier transform to reduce noise interference, monitor voltage fluctuations at the power supply terminal and abnormal harmonic voltage events. If abnormal events are detected, NTP will be used. The timestamp records the time at which the exception event occurred. The direct voltage and current waveform measurement methods presented in this study will be described in Chapter 3. The accuracy of the

measurements will be calculated in Chapter 4, and the analysis of the advantages and disadvantages of using the proposed power quality monitoring method will be given out in Chapter 5.





Chapter 3 Method



This chapter focuses on the experimental methods, research processes and development of power quality sensors. The goal of this study is to establish a reliable and stable power quality monitoring system that can directly measure voltage and current in real time, and the monitoring data can be presented in a waveform on a UI interface. Utilizing the developed IoT-based power quality sensors, the power quality of the power device can be presented in real time. In order to examine the accuracy of the power quality sensor and calibrate the measurement parameters, a highly accurate transient recorder is used to measure power quality parameters, and then the waveforms of the measuring results of both devices are analyzed by the fast Fourier transform (FFT) and examined by the wavelet transform analysis to verify the accuracy of the power quality device proposed in this study.

3.1 Poor Power Quality Event Detection

This study mainly focuses on the detection and processing of transient voltage surges, voltage sags, voltage interruptions and irregular harmonics. The following paragraphs describe the detection methods and application techniques.



3.1.1 Irregular Voltage Events

The IEEE Standard 1159-2009 provides a common terminology to enable the discussion and evaluation of voltage magnitude variations and to define the range of voltage sags, swells, and interruptions. A voltage RMS variation indicator is designed to evaluate the quality of service within a specified power network. The calculation method in the time domain is shown in Eq. (3-1), where V_n is the voltage at the n^{th} point and N is the number of sampling points.

$$RMS_v = \left(\frac{\sum_{n=0}^N V_n^2}{N} \right)^{-1/2} \quad (3-1)$$

This study assumes that the DC offset is 0, so it is ignored. However, because the voltage signal is analyzed in the time domain, it may be interfered by harmonics or noise, resulting in inaccurate analysis results and misjudgment. The FFT can be used to convert a time domain signal into a frequency domain signal. Additionally, it is possible to remove high frequency noise. By summing the energy at each frequency, it can be converted into RMS as shown below. V_n is the integer multiple harmonic component in the spectrum; N is the calculated number of points of the FFT

$$RMS_{v,FFT} = \frac{\left(\sum_{n=1}^k V_n^2 \right)^{-1/2}}{(N/2) \times \sqrt{2}} \quad (3-2)$$

In this equation, k depends on the highest harmonics that the system can measure. The RMS calculated by Eq. (3-2) is used as an indicator for power quality events, and it determines whether a voltage is swelled, sagged, or interrupted. In this study, after calculating the RMS, referring to the IEEE1599-2009 specification, and some thresholds used to determine power events are discussed. When a voltage falls between 0.9 and 1.1 times of the regular value, then the voltage is a regular one; if a voltage exceeds 1.1 times of the regular value, this is called a “voltage swell”; otherwise, a voltage sag occurs if a voltage falls between 0.1 times and 0.9 times of the regular value. Finally, a voltage interruption occurs if the voltage is lower than the standard value of 0.1 times

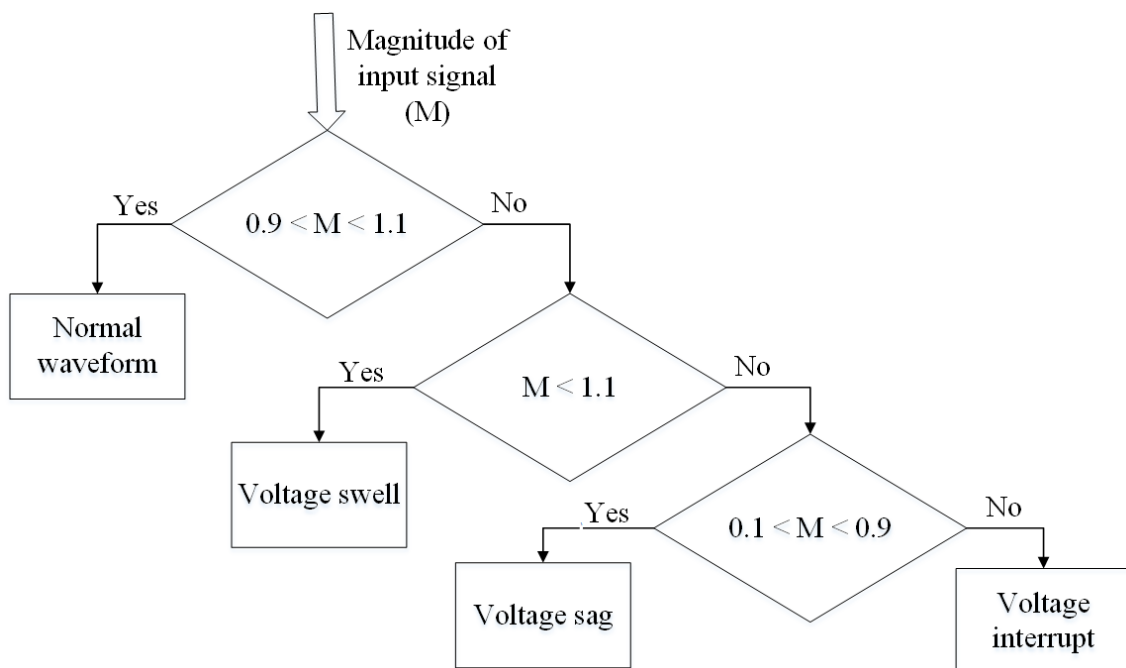


Figure 3-1 The flow chart of the determination of an irregular voltage.



3.1.2 Irregular Harmonic Event

Usually, in order to examine the degree of distortion of the harmonics, the total harmonic distortion (THD) is often used as an indicator for voltage distortion. Therefore, according to the IEEE Std. 519-1992 standard, in this study the THD is set not to exceed 5 %. When the system detects an irregular harmonic event, the system would calculate the THD through the FFT and present the results to users via a visual interface.

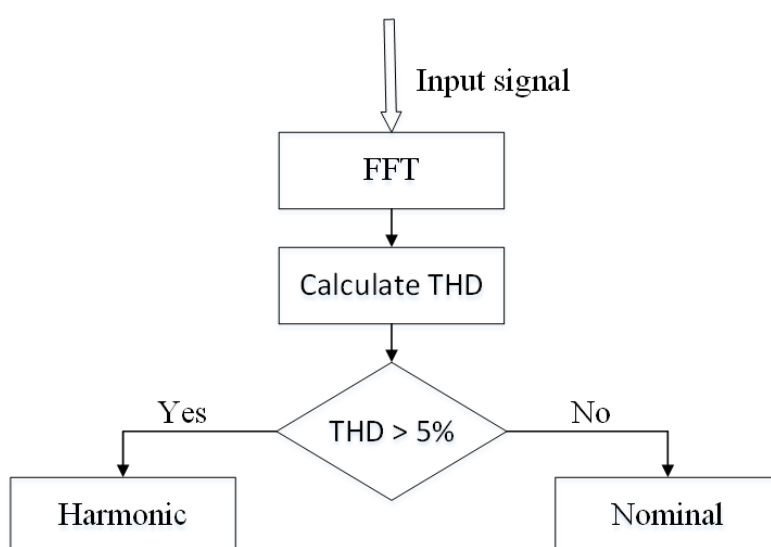


Figure 3-2 The flow chart of determining an irregular harmonic.

3.2 Fast Fourier Transform

The Fourier transform is an integral transform, which is often used to convert signals between the time domain and frequency domain. It can express a signal as a superposition of cosine and cosine functions of different frequencies, which can be used in signal analysis. The transformation reveals feature that are not observable in the time domain or

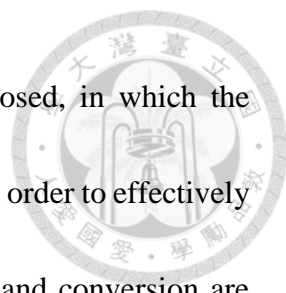
in the frequency domain. In order to implement the Fourier transform calculation in digital signal processing, the continuous function must be discretized, and the Fourier transform of the discrete function is called the discrete Fourier transform. In the digital signal processing, the discrete signal $x(n)$ can be converted into the spectral energy $X[k]$ of the N point by the discrete Fourier transform. The Discrete Fourier transform formula is shown in Eq. (3-3):

$$X[k] = \sum_{n=0}^{N-1} x_n e^{-i2\pi k \frac{n}{N}} \quad (3-3)$$

If N items are directly calculated by the definition of DFT, N^2 complex multiplication and $N(N-1)$ complex addition operations are required, and the time complexity is $O(N^2)$. In practical applications, the Cooley-Tukey algorithm simplifies the operation by the characteristics of periodicity and symmetry of the twiddle factor. The results are shown in Eqs. (3-3) and (3-4) (Cooley and Tukey, 1965). The complexity is reduced from $O(N^2)$ to $O(N \log N)$. This simplified fast algorithm is called the fast Fourier Transform (FFT).

$$e^{-i2\pi k \frac{n}{N}} = e^{-i2\pi(N+k) \frac{n}{N}} \quad (3-4)$$

$$e^{-i2\pi k \frac{n}{N}} = e^{-i2\pi(N+k) \frac{n}{N}} \quad (3-5)$$



In recent years, many measurement methods have been proposed, in which the concept of Fourier series is most common for analyzing harmonics. In order to effectively analyze the harmonic components of power signals, Fourier series and conversion are most effective and direct. The speed of the Fast Fourier Transform calculation is fast, and the method is simple, so it is widely used in many studies. Most of the measuring instruments use fast Fourier transform algorithms. The fast Fourier Transform can be divided into two types: Decimation-In-Time (DIT) and Decimation-In-Frequency (DIF). The DIT regroups items in the DFT formula in the time domain, while the DIF decomposes the frequency domain sequence (Proakis and Manolakis, 1995).

3.2.1 DIT of FFT

The fast Fourier transform with the DIT means that the time domain sequence is grouped according to sequence n . When N is even, it can be divided into odd and even sequences according to the sequence n . Here, a twiddle factor is defined to simplify the expression $W_N^{kn} = e^{-i2\pi kn/N}$. Based on the discrete Fourier transform formula,

$$X[k] = \sum_{n=0}^{N-1} x_n W_N^{kn} \quad (3-6)$$

Then,

$$X[k] = \sum_{n(\text{even})} x[n] W_N^{kn} + \sum_{n(\text{odd})} x[n] W_N^{kn} \quad (3-7)$$



Suppose that the even combination group has $n=2s$, and the odd combination group has $n=2s+1$, thus,

$$\begin{aligned}
 X[k] &= \sum_{s=0}^{(N/2)-1} x[2s]W_N^{2ks} + \sum_{s=0}^{(N/2)-1} x[2s+1]W_N^{(2s+1)k} \\
 &= \sum_{s=0}^{(N/2)-1} x[2s]W_N^{2sk} + w_N^k \sum_{s=0}^{(N/2)-1} x[2s+1]W_N^{2sk} \\
 &= \sum_{s=0}^{(N/2)-1} x[2s]W_{N/2}^{ks} + W_N^k \sum_{s=0}^{(N/2)-1} x[2s+1]W_{N/2}^{sk} \\
 &= G[k] + W_N^k H[k]
 \end{aligned} \tag{3-8}$$

which,

$$G[k] = \sum_{s=0}^{(N/2)-1} x[2s]W_{N/2}^{ks} \tag{3-9}$$

$$H[k] = \sum_{s=0}^{(N/2)-1} x[2s+1]W_{N/2}^{sk} \tag{3-10}$$

where $G[k]$ and $H[k]$ are periodic:

$$G[k + \frac{N}{2}] = G[k] \tag{3-11}$$

$$H[k + \frac{N}{2}] = H[k] \tag{3-12}$$

Taking $N=8$ as an example, the above derivation can be drawn as the following diagram:

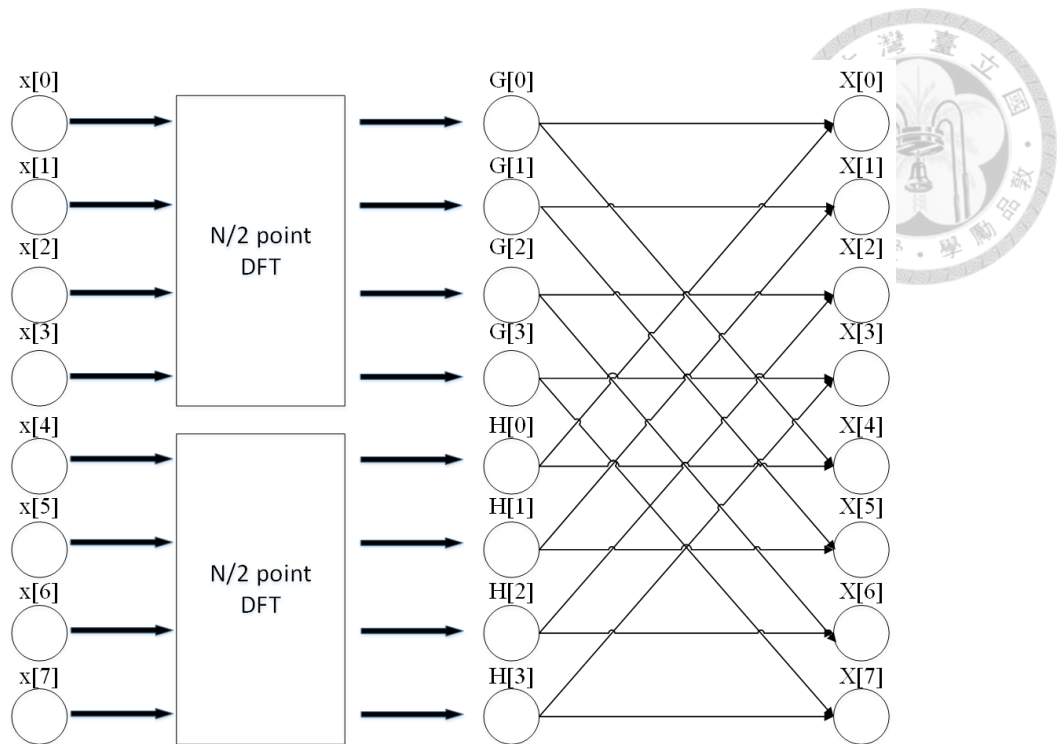


Figure 3-3 Simple 8-point DIT of FFT.

3.2.2 DIF of FFT

The fast Fourier transform with DIF means that the frequency domain sequences are grouped according to sequence k . It can be divided into a pre-sequence and a post-sequence according to sequence n , as shown in Eq. (3-13). Same as the DIT, the DIF is also based on the discrete Fourier transform formula, and

$$X[k] = \sum_{n=0}^{N-1} x_n W_N^{kn} \quad (3-13)$$

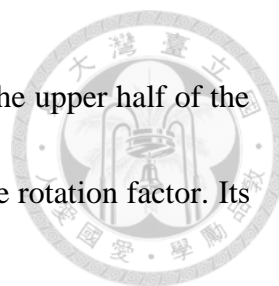
Specially, k points are grouped into even k points and odd k points. First the combination of even k points is observed, assuming $k=2s$, where $r = 0, 1, 2, 3, \dots, (N/2)-1$



$$\begin{aligned}
X[2s] &= \sum_{n=0}^{N-1} x_n W_N^{2sn} \\
&= \sum_{n=0}^{(N/2)-1} x[n] W_N^{2sn} + \sum_{n=N/2}^{N-1} x[n] W_N^{2sn} \\
&= \sum_{n=0}^{(N/2)-1} x[n] W_N^{2sn} + \sum_{n=0}^{(N/2)-1} x[n + (N/2)] W_N^{2s[n+(N/2)]} \\
&= \sum_{n=0}^{(N/2)-1} x[n] W_N^{2sn} + \sum_{n=0}^{(N/2)-1} x[n + N/2] W_N^{2sn} \\
&= \sum_{n=0}^{(N/2)-1} (x[n] + x[n + (N/2)]) W_{N/2}^{sn} \\
&= \sum_{n=0}^{(N/2)-1} g[n] W_{\frac{N}{2}}^{sn}
\end{aligned} \tag{3-14}$$

This is the DFT of the $(N/2)$ point after adding the signals of the upper half and the lower half of the input data. In the combination of odd K points, suppose $k=2s+1$,

$$\begin{aligned}
X[2s+1] &= \sum_{n=0}^{N-1} x_n W_N^{(2s+1)n} \\
&= \sum_{n=0}^{(N/2)-1} x[n] W_N^{(2s+1)n} + \sum_{n=N/2}^{N-1} x[n] W_N^{(2s+1)n} \\
&= \sum_{n=0}^{(N/2)-1} x[n] W_N^{(2s+1)n} + \sum_{n=0}^{(N/2)-1} x[n + (N/2)] W_N^{(2s+1)[n+(N/2)]} \\
&= \sum_{n=0}^{(N/2)-1} x[n] W_N^{(2s+1)n} + \sum_{n=0}^{(N/2)-1} x[n + N/2] W_N^{(2s+1)n} \\
&= \sum_{n=0}^{(N/2)-1} (x[n] - x[n + (N/2)]) W_{N/2}^{(2s+1)n} \\
&= \sum_{n=0}^{(N/2)-1} (x[n] - x[n + (N/2)]) W_{N/2}^{sn} W_N^n \\
&= \sum_{n=0}^{(N/2)-1} (h[n] W_N^n) W_{\frac{N}{2}}^{sn}
\end{aligned} \tag{3-15}$$



This is the DFT of the $(N/2)$ point after subtracting the signal from the upper half of the input data to the lower half of the signal, and the result multiplies the rotation factor. Its signal flow chart is shown in Figure 3-4.

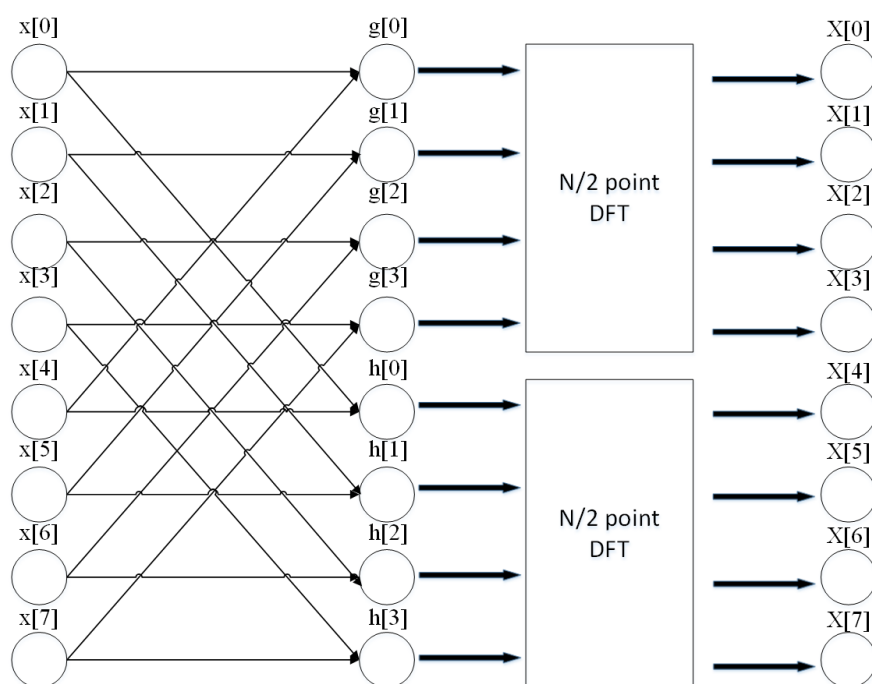
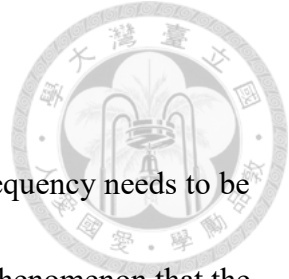


Figure 3-4 Simple 8-point DIF of FFT.

3.2.3 Limitations and Effects of FFT

The fast Fourier transform is a fast algorithm that utilizes the periodicity and symmetry of the rotation factor of discrete Fourier transform. Therefore, the following effects must be avoided when performing a spectrum analysis:



A. Aliasing Effect

According to the Nyquist Sampling Theorem, the sampling frequency needs to be more than twice of the frequency of the signal to be tested. The phenomenon that the spectrum overlaps after the signal is sampled, that is, the frequency component higher than half of the sampling frequency will be reconstructed into a signal lower than half of the sampling frequency, is called the aliasing effect.

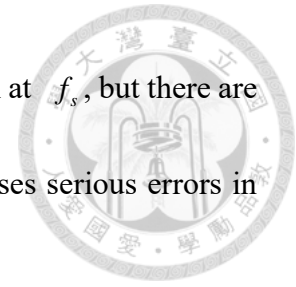
B. Picket-fence Effect

Since the spectral line of the discrete Fourier transform is a discrete value obtained by sampling the continuous spectral function of the Fourier transform, the spectrum can only be observed at a limited frequency. If the spectrum is separated by a large gap, and there is a spectral component that is just between the two lines and cannot be detected. Therefore, the characteristics of the frequency domain are difficult to be fully observed. The interval between the spectral lines is called the spectral scale, and the smaller the spectral scale, the probability of missing the signal becomes smaller.

C. Leakage Effect

For a sinusoidal sequence with a frequency of f_s , its spectrum should only have a discrete spectrum at f_s . If the input data are not an integer multiple of the period of the signal, a discontinuous truncation will occur on the time domain waveform. As

a result, the spectrum of the signal is not only a discrete spectrum at f_s , but there are spectral lines in the frequency band centered on f_s , which causes serious errors in the spectrum. This phenomenon is called the leakage effect.



The aliasing effect can be avoided by using a sampling frequency greater than twice of the frequency of the signal to be tested. To reduce the barrier effect and leakage effect, that Hanning Window and addition the length of the window sequence are the most widely used method. However, this study assumes that the input frequency is fixed at 60 Hz, and the sampling frequency is designed to be an integer multiple of 60 Hz (the sample rate used in this study is 7680 Hz to reduce the leakage effect).

3.3 Wavelet Transform

The standard Fourier transform converts the signal from the time domain to the frequency domain for analysis, but there is no way to know the frequency information of the signal at different time from the frequency domain. Only the frequency components of the signal are known. Therefore, it is not suitable for analyzing a signal whose frequency changes over time. However, compared to the standard Fourier transform, the short-time Fourier transform (STFT) includes a window function to analyze the frequency with time. As the size of the window function varies, there will be different frequency and time resolutions. Taking the square window function as an example, when the width of the window becomes larger,

the resolution of the frequency is better, but the time resolution is decreased. By contrast, when the width of the window becomes smaller, the time resolution becomes the greater, but the frequency resolution becomes lower. However, the size of the finite-length window limits the frequency resolution, but a wavelet transform can solve this problem. A multi-resolution analysis usually gives a better signal representation. Therefore, this study also uses a wavelet transform to perform a series of analyses on the measured waveform data to determine the reliability of the monitoring system. The basic function of the wavelet transform has the characteristics of automatic contraction, the low frequency message using a wide time interval, and the high frequency message using a narrow time interval. Therefore, it can be used to detect the time when an event occurs by using it on the power disturbance.

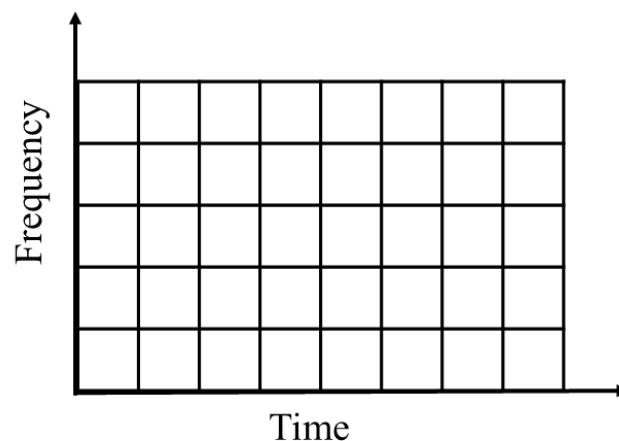


Figure 3-5 Fixed window size of the STFT.

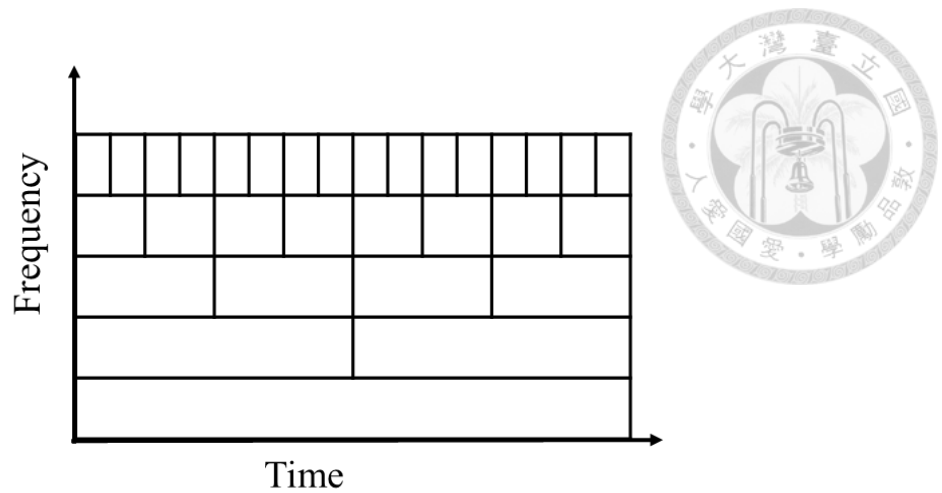


Figure 3-6 Window size of a wavelet.

From the perspective of signal analysis, the principle of the wavelet transform is to represent the original signal in a continuous approximation by different resolution spaces.

In other words, for any signal $x(t) \in L^2(R)$, a set of basic functions $\psi_{a,b}(t)$ can be obtained by dilated and shifted the mother wave $\psi_{a,b}(t)$ (Sabin and Sundaram, 1996).

$$\psi_{a,b(t)} = |a|^{-1/2} \psi\left(\frac{t-b}{a}\right), \quad (b \in R, a > 0) \quad (3-16)$$

in the formula, a is a scaling factor. When $|a| > 1$, the mother wavelet becomes wider and changes slowly, so it corresponds to the low frequency. When $|a| < 1$, the mother wavelet is compressed, has a small degree of support on the time axis, and corresponds to the high frequency, because the mother wavelet is narrowed and the change becomes faster. b is the time-shifting parameter of the mother wave, which is used to determine the position of the mother wavelet. When the mother wave is narrow, the smaller b value should be

selected so that the displacement distance is shorter each time. When the wavelet is wider, the larger the wavelet should be selected. The b value is used to avoid an excessive overlap of displacement. Therefore, the b value has the effect of adjusting the optimal step size of the mother wave on the time axis.

For any function $x(t)$ with continuous time properties and integral characteristics , its continuous wavelet transform (CWT) is defined as follows:

$$CWT(a,b) = |a^{-1/2}| \int_{-\infty}^{\infty} x(t) \psi\left(\frac{t-b}{a}\right) dt \quad (3-17)$$

According to the difference in characteristics of power quality events, the mother wave (Db4) of Daubechies wave element with eight coefficients was selected to analyze the power quality events. The Daubechies mother wave is defined by a scaling function $\phi(x)$ (Narcowich and Boggess, 2009):

$$\phi(x) = \sum_{k=0}^{N-1} a_k \phi(2x-k) \quad (3-18)$$

Where a_k is a square power sequence, and the Daubechies mother wave can be defined as

$$\psi(t) = \sum_{k=0}^{M-1} b_k \phi(2x-k) \quad (3-19)$$

Also, b_k is a square power sequence. However, the voltage and current signals measured in this study are discrete signals, so discrete wavelet transform must be used in signal conversion to obtain accurate analysis results.

The wavelet transform of the original signal $C_{0,L}[n]$ can be decomposed into two sub-band signals $D_{1,H}[n]$ and $C_{1,L}[n]$ by using a set of high-pass filter $h[n]$ and low-pass filter $g[n]$, and a first-order wavelet transform diagram is shown in Figure 3-7.

After $C_0[n]$ and $h[n]$ are subjected to the convolution operation, the down-sampling filter ($\downarrow Q$) is performed, and here is an example $Q=2$. That is, take the part of its even point to get $C_{1,L}[n]$, Similarly, $D_{1,H}[n]$. In the opposite way, the high and low frequency sub-signals are up-sampling ($\uparrow 2$) through the high pass filter and low-pass filter, then the original signal can be obtained, as shown in Figure 3-8.

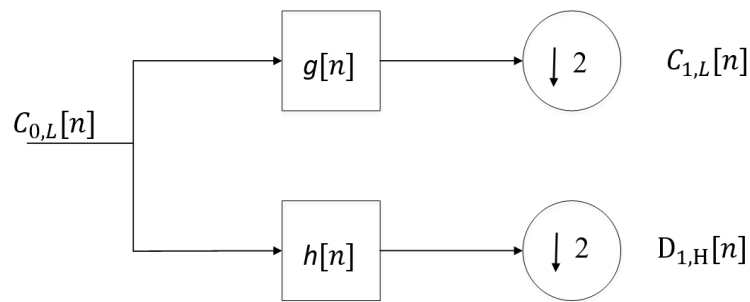


Figure 3-7 The decomposition diagram of the first order wavelet transform.

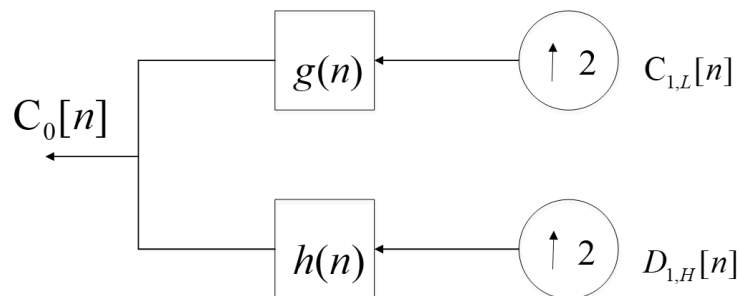
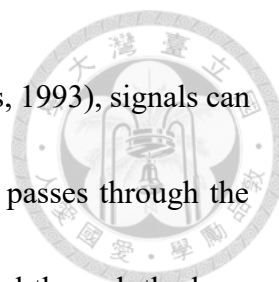


Figure 3-8 The composition diagram of the first order wavelet transform.



Using the concept of Multi-resolution Analysis (MRA) (Douglas, 1993), signals can be parsed or reconstructed at different resolution levels. The signal passes through the high-pass filter to obtain the high-band signal message, and the signal through the low-pass filter contains the low-band message, and then the low-band message continues to be decomposed downward. The analysis of each stage can pass through the high-low-pass filter. By splitting out messages in different sub-bands, the signal can be processed by MRA to realize the characteristics of the transient signal on the time axis and the signal energy in different sub-bands, so that the harmonics, flicker, interruption, and pressure rise, gut the voltage drops, and other signals can be detected accurately (Brito, *et al.*, 1998; Daubechies, 1990).

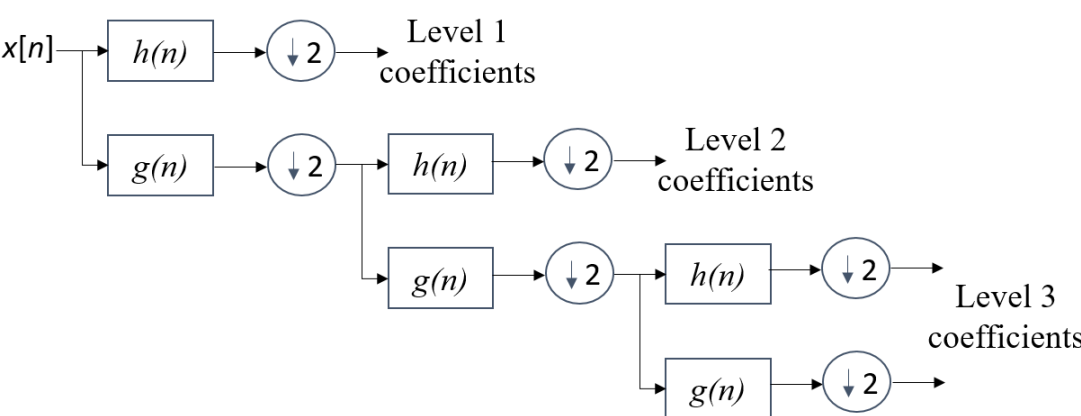


Figure 3-9 Discrete signal as layer α in the discrete wavelet transform architecture.

And the layer α in the architecture can be represented as:

$$C_{\alpha,L}[n] = \sum_{k=0}^{k=1} C_{\alpha-1,L}[2n-k]g[k] \quad (3-20)$$

$$D_{\alpha,H}[n] = \sum_{k=0}^{k=1} D_{\alpha-1,L}[2n-k]h[k] \quad (3-21)$$



3.4 Power Quality Monitoring System

In this study, the target power equipment is the OMICRON CMC 356, which is a universal relay test set and commissioning tool. The device used to examine the performance of the power quality monitoring system is based on the Internet of Things technology, as shown in Figure 3-10. A schematic of the sensor mounted on the OMICRON CMC 356 is shown, which provides basic information about how the mount of the sensor. Figure 3-11 shows a flow chart for the establishment and verification of the proposed power quality monitoring system. The voltage and current output from the CMC356 are measured using a commercially available power quality transient recorder. The measured data are compared to the actual values measured by the power quality sensor. The performance of the power quality monitoring system is examined by analyzing the actual measurement results using the fast Fourier transform and wavelet transform. After that, power companies can benefit from real-time monitoring information and display. In addition, the proposed system can work with GIS systems to increase their viability and practicality. Figure 3-12 shows the architecture of a power

quality monitoring system. The voltage and current data at the end of the sampling are transmitted to a database that outputs the power quality results for a particular power device. These results can be provided to the utility company to improve the stability of the transmission network or as power dispatch reference.



Figure 3-10 Appearance of the IoT-based PQ sensor.

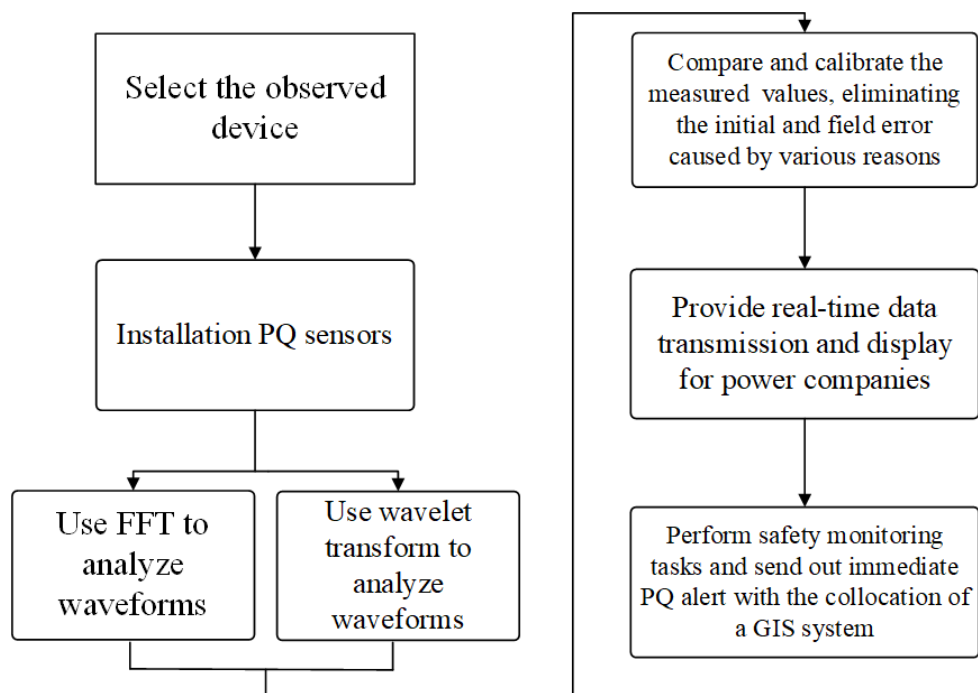


Figure 3-11 System flowchart.

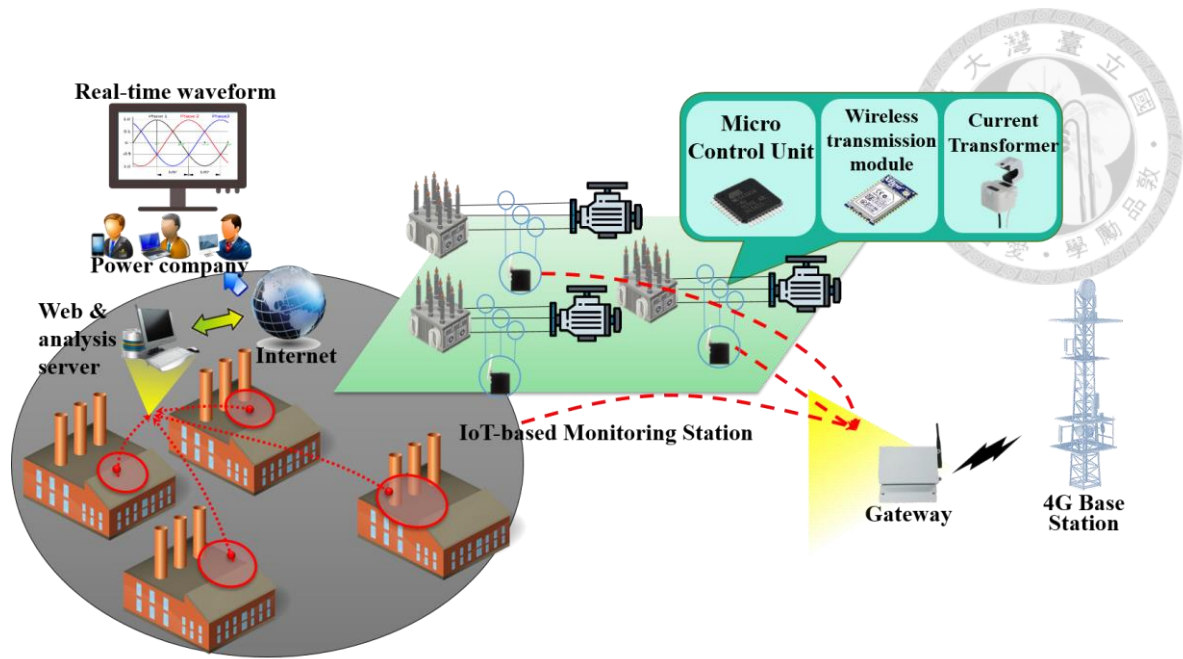


Figure 3-12 System architecture.

The power quality sensor proposed in this study is mainly composed of a microcontroller, a wireless transmission module, a current sensor and sensing circuits.

A. Microcontroller

A microcontroller is a microcomputer that integrates a central processing unit, a memory, a timer/counter, various input/output interfaces, etc. All of the components are integrated into an integrated circuit chip. Compared with general-purpose microprocessors used in personal computers, such a microcontroller emphasizes self-supply (without requiring external hardware) and cost savings. Its greatest advantage is its small size, which can be placed inside many instruments.

The microcontroller used in this study has a control chip of ATmega32u4, an 8-bit Microcontroller with 132k bytes of ISP Flash and a USB controller. It also contains a processing chip that converts the analog signal into a digital signal, and the resolution of this ADC is 10 bits. The sampling frequency of the signal is about 9.6 kHz.

Table 3-1 Specifications of the MCU.

Name	Value
Program Memory Type	Flash
Program Memory Size (KB)	32
CPU Speed (MIPS/DMIPS)	16
SRAM Bytes	2560
Data EEPROM/HEF (bytes)	1024
Digital Communication Peripherals	1-UART, 2-SPI, 1-I2C
Capture/Compare/PWM Peripherals	2 Input Capture, 2 CCP, 12PWM
Timers	2 x 8-bit, 2 x 16-bit
Number of Comparators	1
Number of USB Modules	1, Full Speed
Temperature Range (°C)	- 40 to 85
Operating Voltage Range (V)	2.7 to 5.5
Pin Count	44

B. Current transformer

In this research, a current transformer (CT) is used as a current sensor, and a CT is a type of transformers, which is mostly used to measure AC. It inputs a current

in its primary, and a current proportional to it is in its secondary. It is mounted on the output end of the inverter device to sense the current after the output, and then a suitable resistor is used to convert its current signal into a voltage signal that can be received by the microcontroller. These signals are finally presented through a user visual interface to show the operation of the device. The type of flow comparator selected in this study is an SCT-16, and the details regarding product specifications are described as follows:

Table 3-2 Specifications of the CT

Name	Value
Applicable current range	150A (7.5~180A Max)
Accuracy	CLASS 0.5 , $RL \leq 6.66 \Omega$
Maximum allowable current	120A RMS continuous
Number of secondary coil turns	3000 ± 2 turns
Secondary Output at Rated Current	333 mV(Resistor inside The CT)
Construction	nylon housing simple lock type
Protection Level	7.5 V (Peak)
Withstand voltage	4KV / 5mA / 1 minute
Insulation resistance	DC 500V / 100 M Ω
Operating temperature	- 40 ~ 65°C
Storage temperature	- 45 ~ 85°C



Figure 3-13 Appearance of the CT (Source:

<http://www.thic.net/?go=product&cid=30>)

C. Wireless transmission module

Wireless communication is a communication method that uses the characteristics of electromagnetic wave signals to propagate in free space for information exchange. There are many advantages of using wireless communication technology, such as low costs and no need to establish physical lines. Moreover, wireless communication is not limited by an industrial environment, and it has strong ability to resist environmental changes, and fault diagnosis is relatively easy. Compared with traditional wired communication, wireless network maintenance can be completed through remote diagnosis and control, which is more convenient and flexible. Wireless networks are also not subject to a particular type of terrain, and when environment change, they can adapt to the new environment with only a few

adjustments. In recent years, short-range wireless communication standards with wider applications and good development prospects have been proposed, including ZigBee, Bluetooth, ultra wideband (UWB) and Wi-Fi. Different from the Bluetooth transmission technology used in other studies (Luis Morales-Velazquez et al., 2017), this study uses the wireless transmission technologies developed by Lee et al. (Lee et al., 2007) to conduct a series of experiments and comparisons. Based on the results, this study selects the ZigBee transmission technology as the transmission protocol, due to its lower power consumption and longer transmission distances.

Standard	Bluetooth	UWB	ZigBee	Wi-Fi
IEEE spec.	802.15.1	802.15.3a *	802.15.4	802.11a/b/g
Frequency band	2.4 GHz	3.1-10.6 GHz	868/915 MHz; 2.4 GHz	2.4 GHz; 5 GHz
Max signal rate	1 Mb/s	110 Mb/s	250 Kb/s	54 Mb/s
Nominal range	10 m	10 m	10 - 100 m	100 m
Nominal TX power	0 - 10 dBm	-41.3 dBm/MHz	(-25) - 0 dBm	15 - 20 dBm
Number of RF channels	79	(1-15)	1/10; 16	14 (2.4 GHz)
Channel bandwidth	1 MHz	500 MHz - 7.5 GHz	0.3/0.6 MHz; 2 MHz	22 MHz
Modulation type	GFSK	BPSK, QPSK	BPSK (+ ASK), O-QPSK	BPSK, QPSK COFDM, CCK, M-QAM
Spreading	FHSS	DS-UWB, MB-OFDM	DSSS	DSSS, CCK, OFDM
Coexistence mechanism	Adaptive freq. hopping	Adaptive freq. hopping	Dynamic freq. selection	Dynamic freq. selection, transmit power control (802.11h)
Basic cell	Piconet	Piconet	Star	BSS
Extension of the basic cell	Scatternet	Peer-to-peer	Cluster tree, Mesh	ESS
Max number of cell nodes	8	8	> 65000	2007
Encryption	E0 stream cipher	AES block cipher (CTR, counter mode)	AES block cipher (CTR, counter mode)	RC4 stream cipher (WEP), AES block cipher
Authentication	Shared secret	CBC-MAC (CCM)	CBC-MAC (ext. of CCM)	WPA2 (802.11i)
Data protection	16-bit CRC	32-bit CRC	16-bit CRC	32-bit CRC

Figure 3-14 Comparison of different wireless transmission protocols (Lee, *et al.*, 2007) .

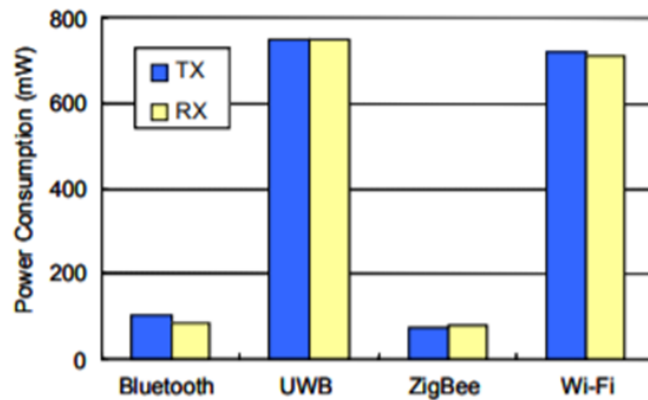


Figure 3-15 Comparison of the power consumption for each transmission protocol (Lee, *et al.*, 2007) .

Therefore, a module for wireless transmission of data is developed, which follows the IEEE 802.15.4 and ZigBee communication protocol. The module is characterized by easy connection and low power consumption. With the ZigBee technology, the star topology can be supported, and the sensing data from the same area can be collected and transmitted through only one gateway.



Figure 3-16 ZigBee wireless transmission module. (Source:

<https://www.seeedstudio.com/Xbee-ZigBee-SMT-250kbps-1200m-RF-Module-w-U-FI-Antenna-Connector-XB24CZ7UIS-004-p-1966.html>)



D. Sensing circuits

In this study, the Altium Designer is used to draw the sensing circuit board. The Altium Designer is an electronic design automation software, supporting for the schematic, PCB, and FPGA design. The software is used to integrate the microcontroller, wireless transmission module, sensor, voltage and current sensing circuit, which is important to the power quality sensor.

The voltage and current waveforms are measured by the following circuit. Through this circuit, the current is converted into a voltage signal by a CT through a burden resistor. After using the input voltage (5 V) of the MCU, the voltage at the intermediate point is 2.5 V, and the 2.5 V is used as the zero point of the waveform, so that the current sensing value can be oscillated between 0 and 5 V.

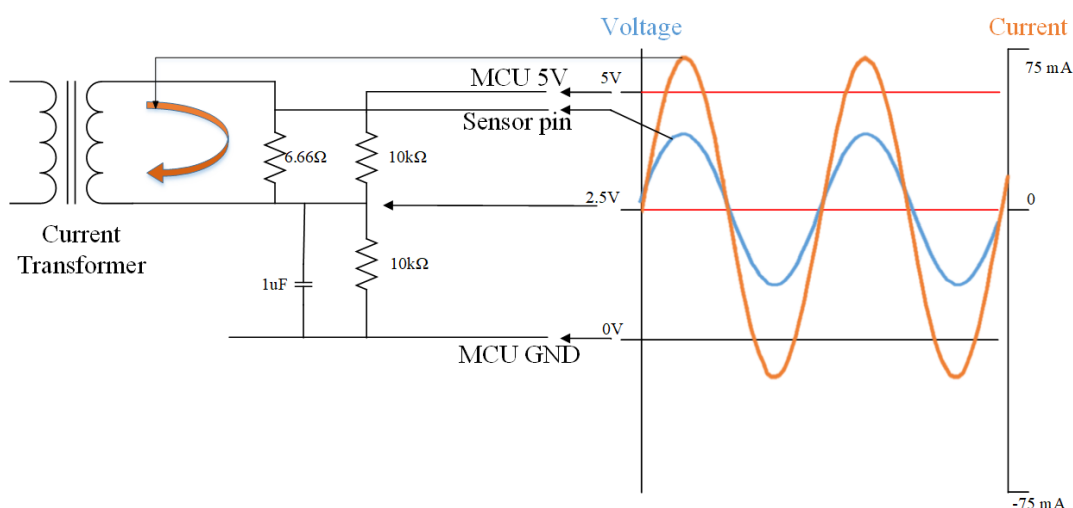


Figure 3-17 Principle of the sensing circuit.



The choice of Burden resistors can be obtained by the following formula:

$$Burden(\Omega) = (V_R * T) / (2\sqrt{2} * A_m) \quad (3-22)$$

where V_R is the inputs voltage of the MCU; T is the number of turns of the CT coil;

and A_m is the maximum current which is chosen as the upper bound of the current range to be measured.

The microcontroller connects the sensor through an analog sensing pin, the voltage and current waveform output can be directly measured by the electronic device, and the microcontroller can then communicate with the wireless transmission module through T_X (data transmission pin) and R_X (data reception pin) pins. Finally, using the gateway to transmit the data back to the database via 4G technology.

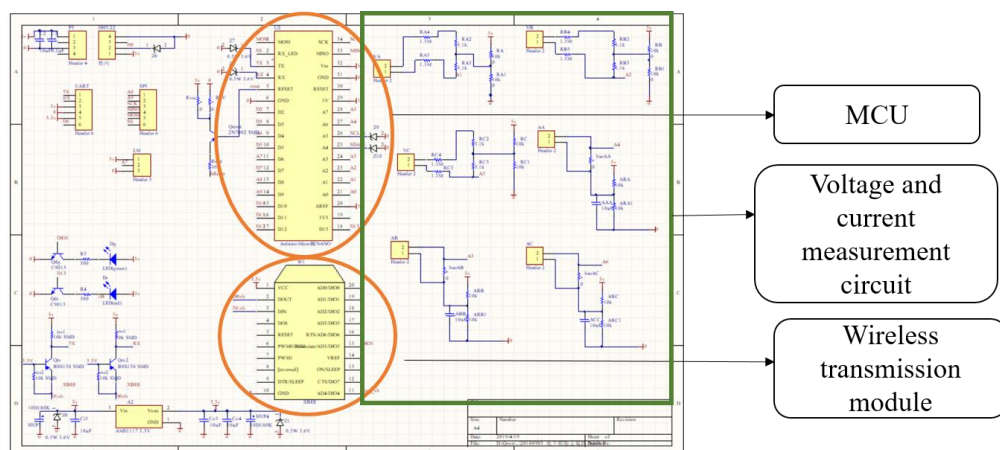


Figure 3-18 Circuit diagram of PQ sensor.

3.5 Network Time Protocol (NTP)

When a bad power quality event occurred, users need to know when the event occurred. Some research papers use GPS to achieve this goal. However, GPS is limited indoors (Huang et al., 2016). Therefore, this study uses the timestamp in the NTP to record the timestamp of the irregular event. The NTP is a network protocol that synchronizes clocks and packet-switched computer systems with variable latency. So as long as there is a network, the NTP can be used.



Chapter 4 Results and Discussion



Chapter 4 describes the comparison between the commercially available transient recorder and the power quality monitoring system proposed in this study for FFT and wavelet conversion. Section 4.1 shows the power quality simulator for system verification. Section 4.2 shows the difference in the accuracy of the sampling points of the monitoring system and the comparison between the instrument and the system after using FFT analysis under good power quality. Section 4.3 describes the measurement results of the proposed power quality monitoring system under adverse power quality events (voltage events and harmonic events) and compares the measurements with commercially available instruments. The analysis was verified as a monitoring system in this study. Section 4.4 shows the feasibility of a large-scale implementation that includes data from several power quality sensors. One of the main goals of this study is to develop an IoT-based power quality monitoring system that can be applied to large-scale monitoring. Section 4.5 shows the user visual interface and the early warning system for event determination.

4.1 Relay Testing System

This experiment uses OMICRON CMC 356, which is a universal relay test set and commissioning tool. There are six current and four voltage output channels are

continuously and independently adjustable in amplitude, phase and frequency. And it is used to simulate power quality abnormal events such as voltage swells, voltage sags and harmonics, etc., through simulation script settings. The abnormal power quality events it can generate are as follows:

1. Power frequency
2. Magnitude of supply voltage
3. Flicker
4. Supply voltage sags and swells
5. Voltage interruptions
6. Transient voltages
7. Supply voltage unbalance
8. Voltage (current) harmonics
9. Voltage (current) interharmonics
10. Rapid voltage changes

The appearance of CMC 356 is shown in Figure 4-1. It is used to output three-phase AC power, and sets the output voltage, frequency, event duration and initial phase angle. The output power is up to 64 A / 860 VA (single phase), and the voltage can be output between 0 and 600 V.



Figure 4-1 OMICRON CMC 356. (Source:

<https://www.omicronenergy.com/cn/products/cmc-356/>)

4.2 System Verification

In order to find an appropriate sensing sampling rate in the allowable operating frequency range of the microcontroller, different sampling frequencies are used in this section to obtain a waveform of one cycle, and perform FFT analysis to confirm whether the result is the same frequency as the output side of the power equipment obtained. This study is based on the measurement of Taiwan's 110 V fundamental frequency 60 Hz as a benchmark; it consists of several functions, namely digital signal measurement, analysis, and user-visible interface. To confirm whether the result is the same as the frequency on the output side of the power equipment.

First, the system uses 960 Hz sampling frequency to measure the waveform of one cycle, and then performs FFT analysis on the result. Second, the system uses 1920 Hz to measure the waveform of one cycle, and then also performs FFT analysis on the result.

Third, the sampling frequency 3840 Hz is used to measure the waveform, and then performs FFT analysis on the result. Finally, the sampling frequency 7680 Hz also to be used to verify how the sampling frequency is suitable for the system. And the result is shown below.

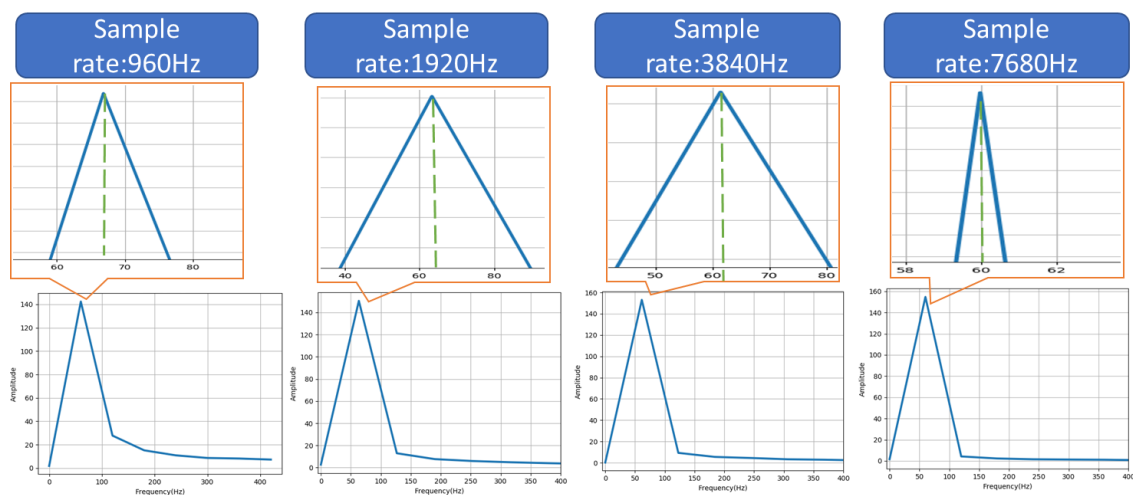


Figure 4-2 Different sampling frequencies of the PQ sensor.

It can be seen from the Figure 4-2 that at the sampling frequency of 960 Hz, the result of the FFT analysis is not as expected. The frequency where the peak appears is not 60 Hz, so the 960 Hz does not provide sufficient accuracy, so the system does not adopt. The same as the sampling frequency of 960 Hz, where the peak occurs, the frequency is not 60 Hz, so the 1920 Hz system is not used. Although the frequency of the highest peak of the sampling frequency of 3840 Hz occurs around 60 Hz, but it is not exactly falling

on 60Hz so the system does not adopt. At last, when the sampling frequency is 7680 Hz, the peak after FFT falls exactly at 60 Hz and no other frequency peaks appear. Therefore, the system uses this sampling frequency. This result is exactly in accordance with the sampling theorem. The sampling theorem shows that the higher the sampling frequency, the more accurate the results are.

After determining the sampling frequency selected by the system, the system and the commercially available transient recorder will measure different power quality events, and then verify the power quality monitoring system after performing FFT on these measurements. This section first outputs from the CMC356 with normal power quality, allowing both systems to measure simultaneously. Other poor power quality event verifications will be discussed separately in the next section.

The measurement results of the time domain waveform in three cycle are shown in Figure 4-3 below.

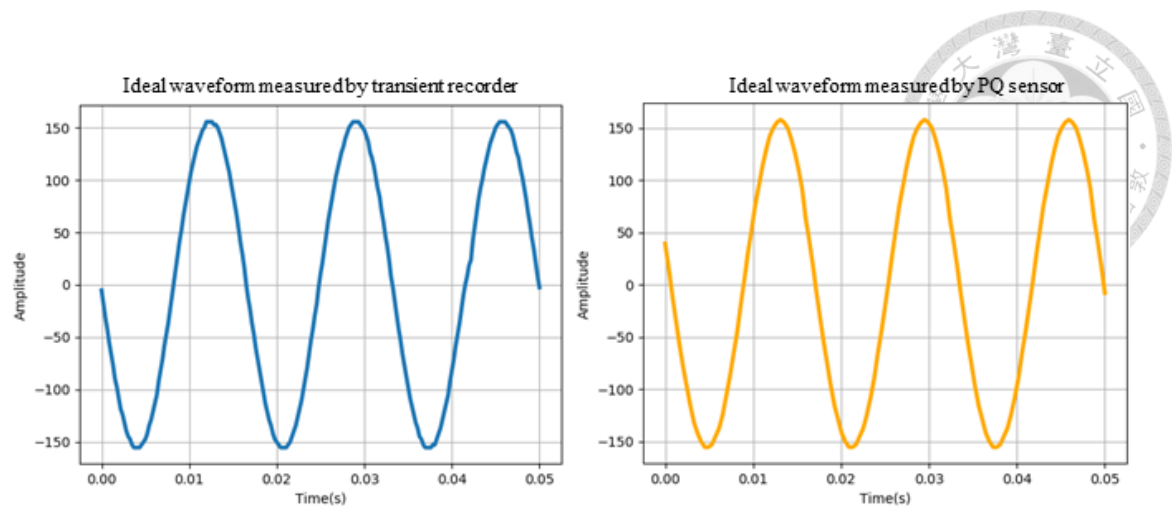


Figure 4-3 Sampling results of different instruments under ideal waveform.

There is no significant difference in the time domain waveform results from the appearance of the two. After the two measurement results are as FFT analysis, the results are as follows:

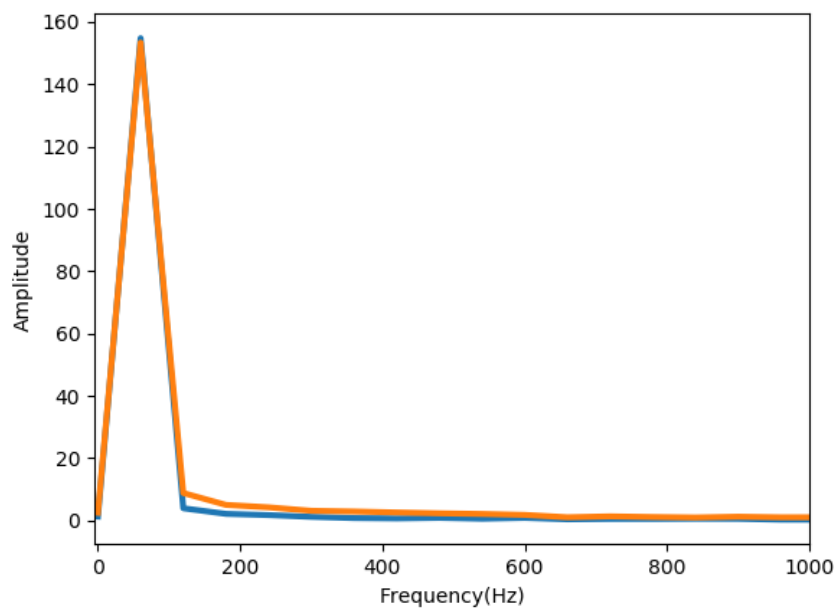
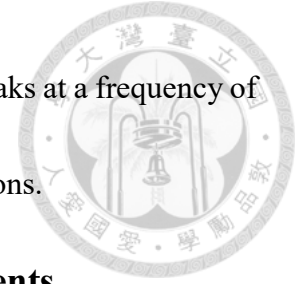


Figure 4-4 Comparison of ideal waveforms after FFT.

Judging from the superposition condition, both of them have peaks at a frequency of 60 Hz, so the system is credible under normal power quality conditions.



4.3 Verify the System with Poor Power Quality Events

This section focuses on re-voltage surges, voltage dips, voltage interruptions, and harmonics. These poor quality power events are measured by commercially available transient recorders and the system. These measurements are then FFT and Discrete Wavelet Transform. The results of the analysis are compared to verify the system reliability. In addition, this study also quantifies these similarities by correlation coefficient and root mean square error (RMSE).

4.3.1 Voltage Swell

In the experiment, using CMC356, through the script writing, the voltage normal value is set to 110 V, the voltage swell value is set to 160 V, and the script operation mode is 110 V normal output 0.1 second, swell to 160 V for 0.1 second, and then return to normal value for 0.1 second. The total time is 0.3 seconds, and the 18-cycle waveforms will be measured. The time domain waveform of the measurement is as shown in Figure 4-5.

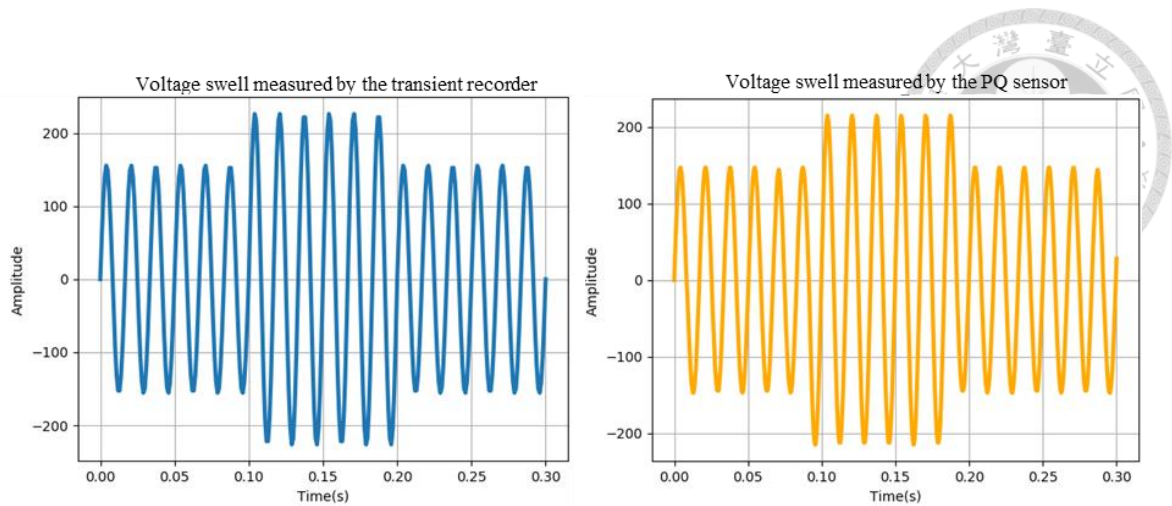


Figure 4-5 Sampling results of different instruments under voltage swell.

It can be seen from the above figure that there is not much difference between the measured time domain waveforms. The results of the two waveforms can be seen through the FFT. The two have a high degree of overlap at a frequency of 60 Hz. Also, the correlation coefficient and root mean square error of this case are 0.9987 and 0.7329, respectively; In the part of wavelet transform, the mother wave used is db4, and the five-level analysis is performed. It can be seen from the analysis result that the first layer has the same trend. The latter layers, because the sampling frequency is not the same, cause the trend to look similar, but inconsistent. The result of the wavelet conversion is also shown in Figure 4-6.

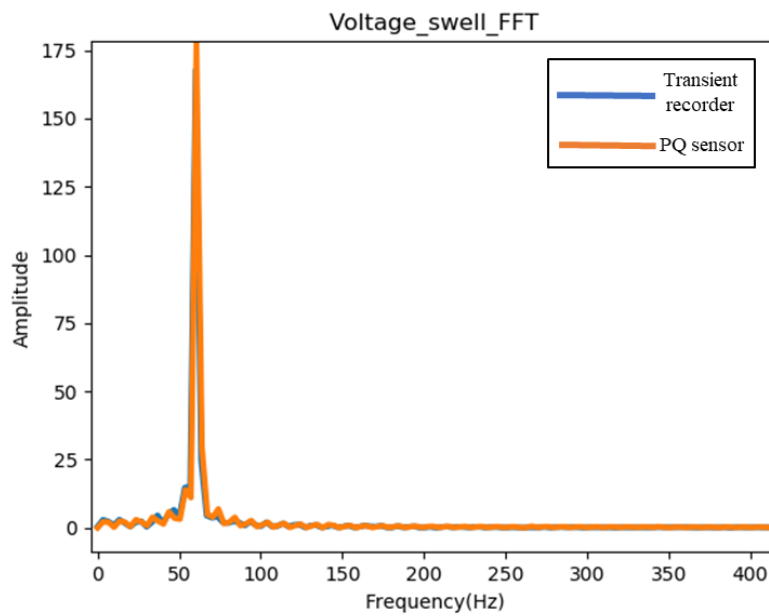


Figure 4-6 Comparison of voltage swell after FFT.

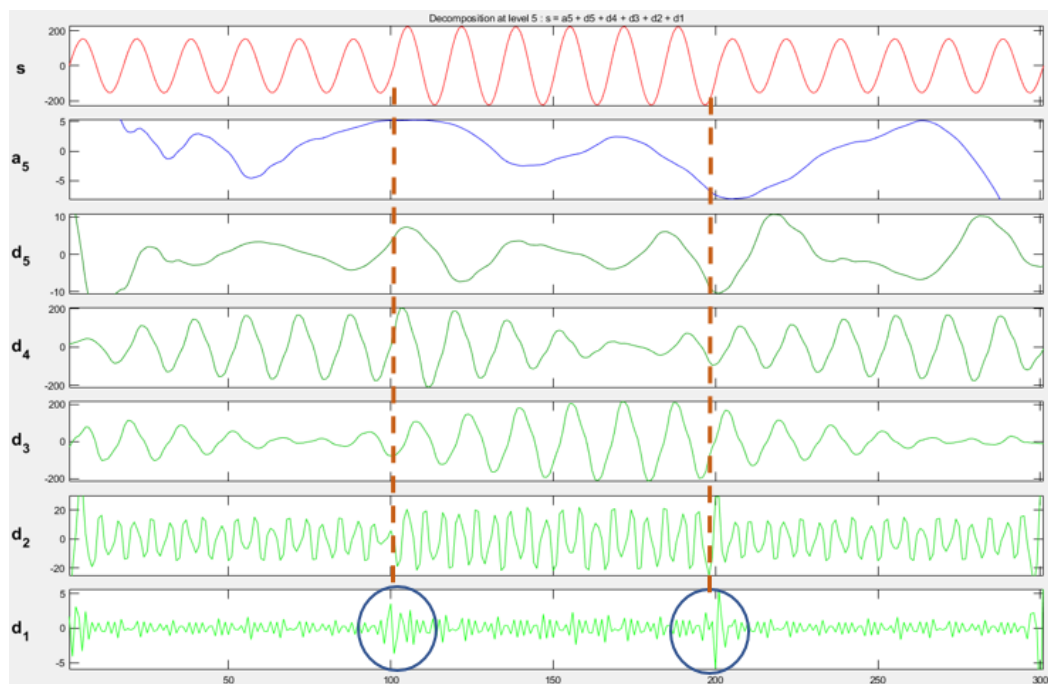


Figure 4-7 DWT results of the voltage swell via the recorder..

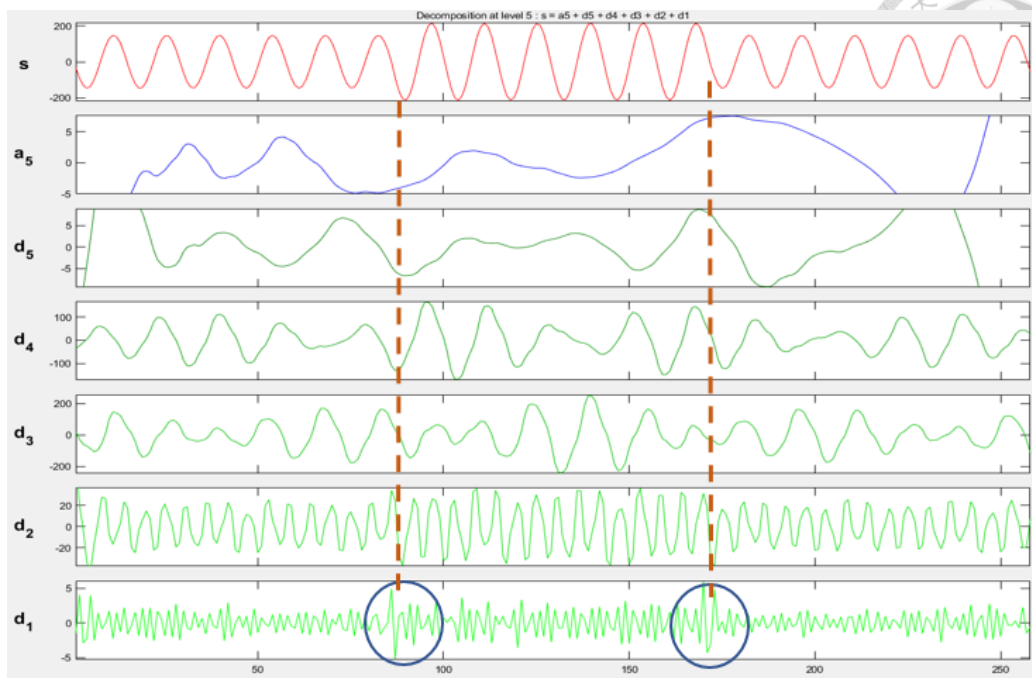


Figure 4-8 DWT results of the voltage swell via the PQ sensor.

4.3.2 Voltage Sag

In the part of the voltage sag, this study will set the voltage normal value to 110 V and the voltage dip value to 80 V. The script operation mode is: 110 V normal output 0.1 seconds, sag to 80 V for 0.1 seconds, and then return to the normal value for 0.1 seconds. The total time is 0.3 seconds, and the 18-cycle waveforms will be measured. The time domain waveform of the measurement is as shown in Figure 4-9.

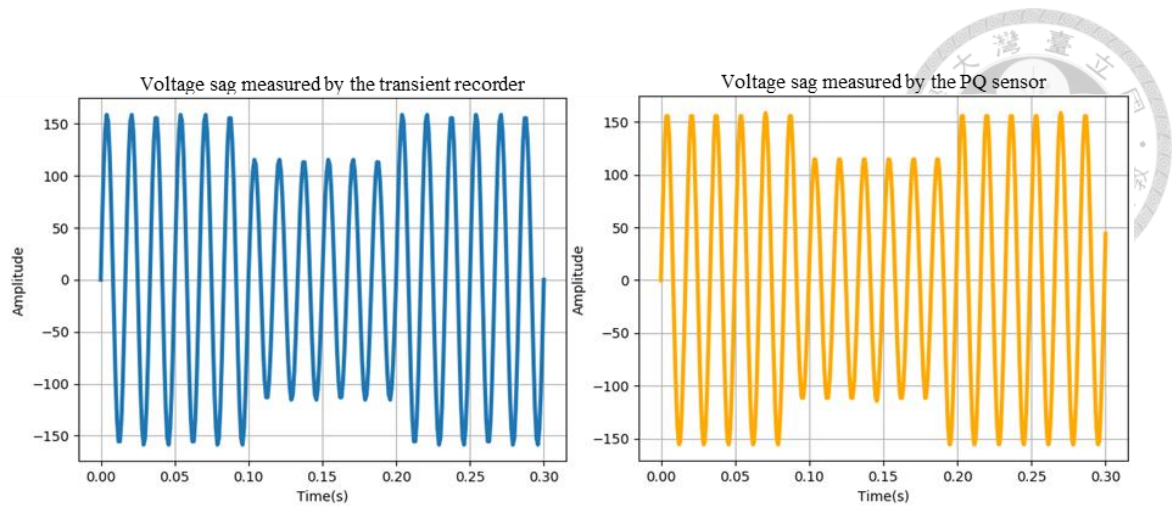


Figure 4-9 Sampling results of different instruments under voltage sag.

A similar conclusion can be obtained from the above figure. It can be seen from the results of the FFT conversion that the two frequencies have a high degree of overlap at a frequency of 60 Hz. And the correlation coefficient is 0.9987, also the value of RMSE is 0.5772; in the part of the wavelet transform, the same trend occurs in the first layer analysis, and The latter layers are also different because the sampling frequency is different, so the trend looks similar but inconsistent.

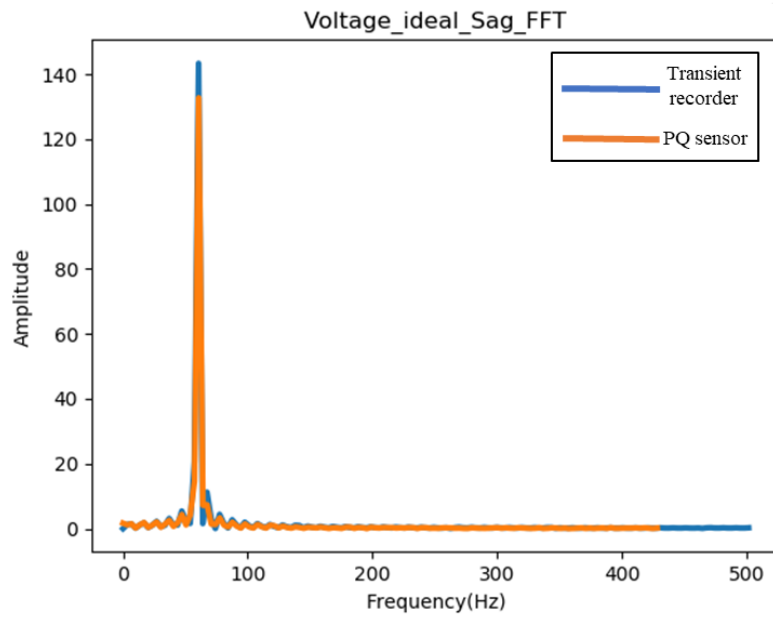


Figure 4-10 Comparison of voltage sag after FFT

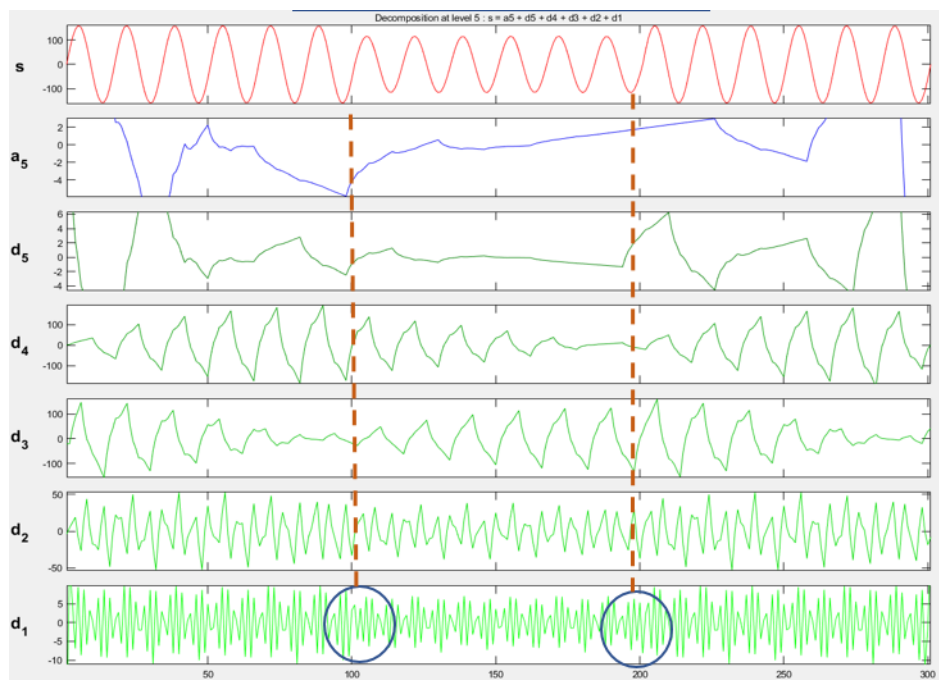


Figure 4-11 DWT results of the voltage swell via the recorder

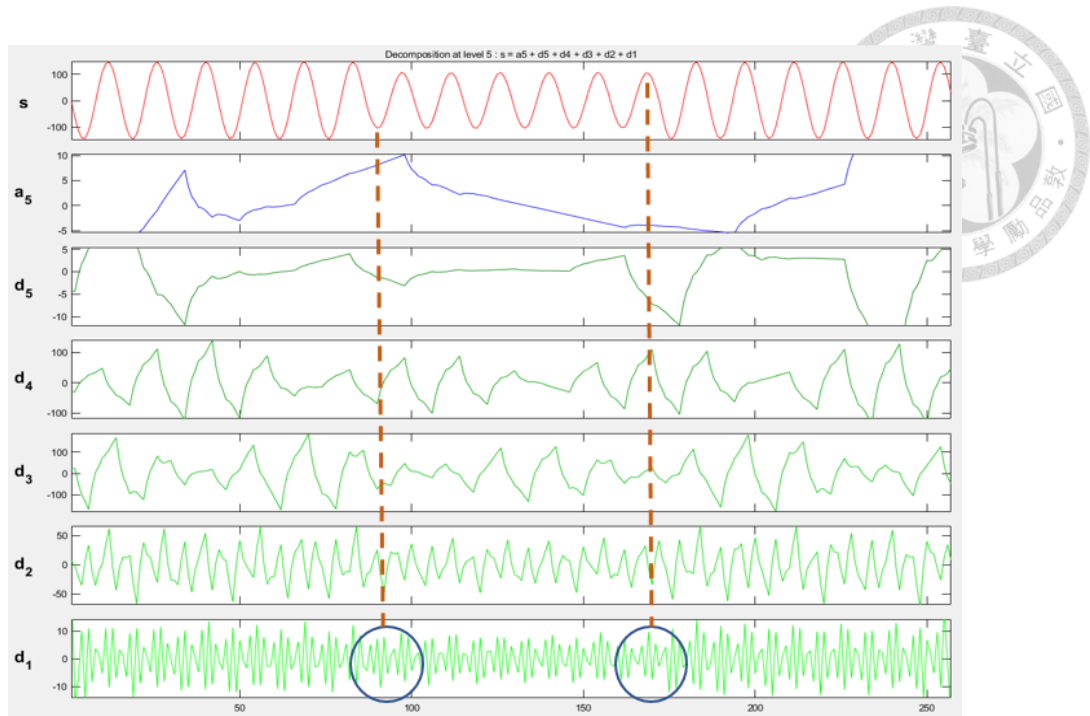


Figure 4-12 DWT results of the voltage sag via the PQ sensor

4.3.3 Voltage Interruption

In the part of voltage interruption, this study will set the voltage normal value to 110 V and the voltage interruption value to 0 V. The script operation mode is: 110 V normal output 0.1 seconds, interruption for 0.1 seconds, and then return to normal value for 0.1 seconds. The total journey is 0.3 seconds, and the 18-cycle wave will be measured. The measured time domain waveform is shown in Figure 4-13.

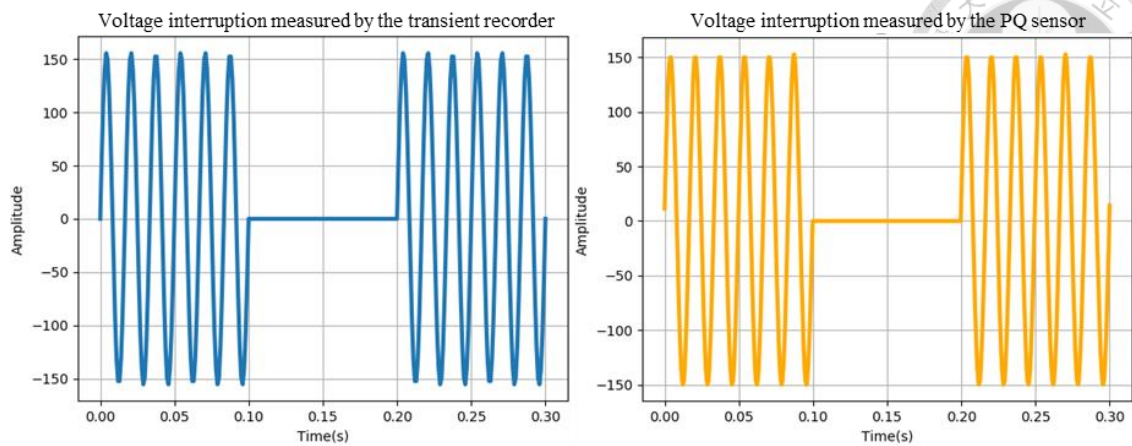


Figure 4-13 Sampling results of different instruments under voltage interruption

The results obtained in the FFT are the same as the above two events, with peaks occurring at 60 Hz and high overlap. The correlation coefficient is 0.9981 and the RMSE value is 0.6155; while the characteristics of voltage interruption are very obvious in wavelet transform, the analysis results are very similar at each level.

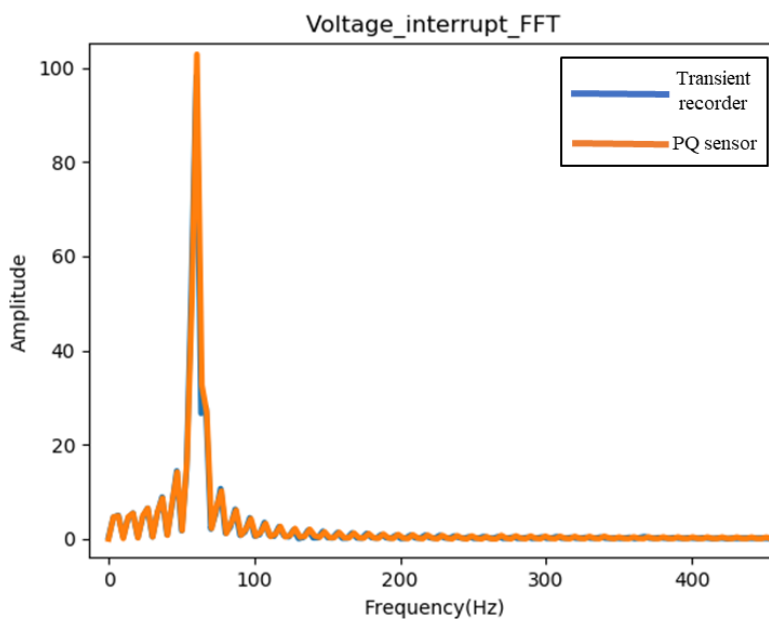


Figure 4-14 Comparison of voltage interruption after FFT.

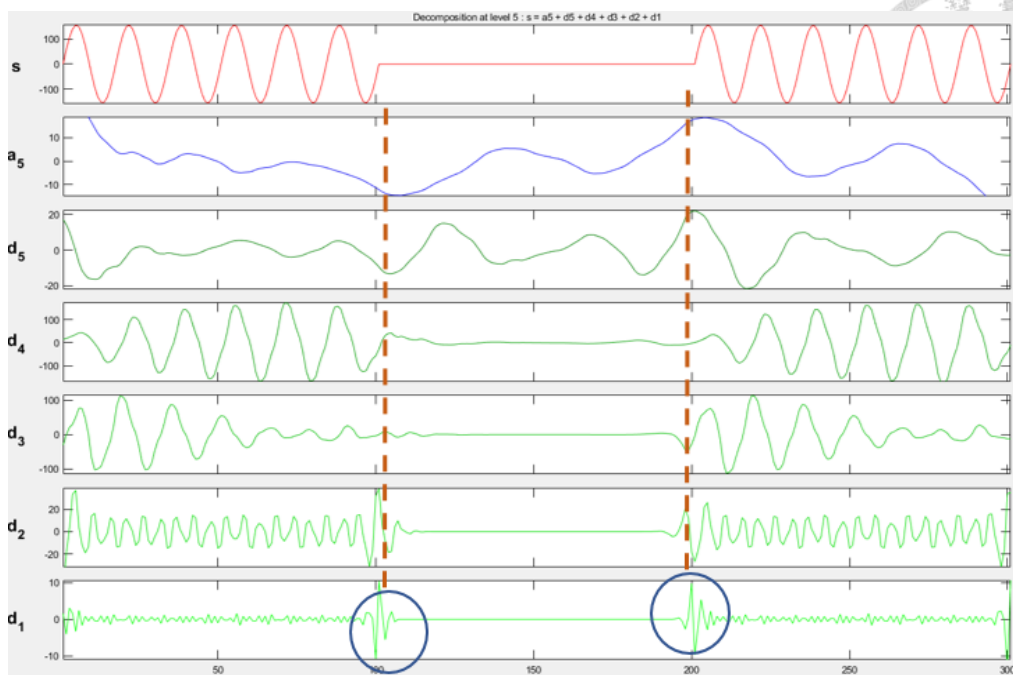


Figure 4-15 DWT results of the voltage interruption via the recorder.

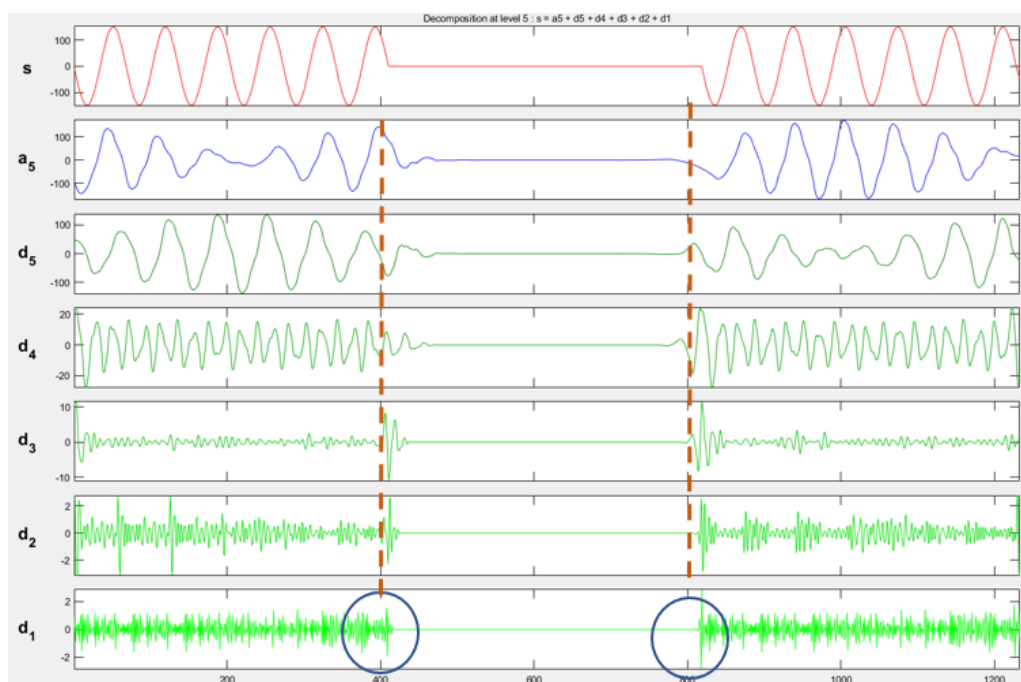


Figure 4-16 DWT results of the voltage interruption via the PQ sensor.



4.3.4 Harmonics

Voltage and current harmonics are also common poor power quality events, so it is also one of the necessary functions of this power quality monitoring system to accurately determine harmonics. In the case of a fundamental frequency of 60 Hz, this study simulates three kinds of voltage harmonics. In different cases, FFT analysis and wavelet analysis are performed via PQ sensor and transient recorder to verify the reliability of the system. In the first case, 50 % of the triple fundamental frequency (180 Hz) harmonics are set. As shown in Figure 4-17, a total of three cycles of harmonic waveforms are measured by two devices.

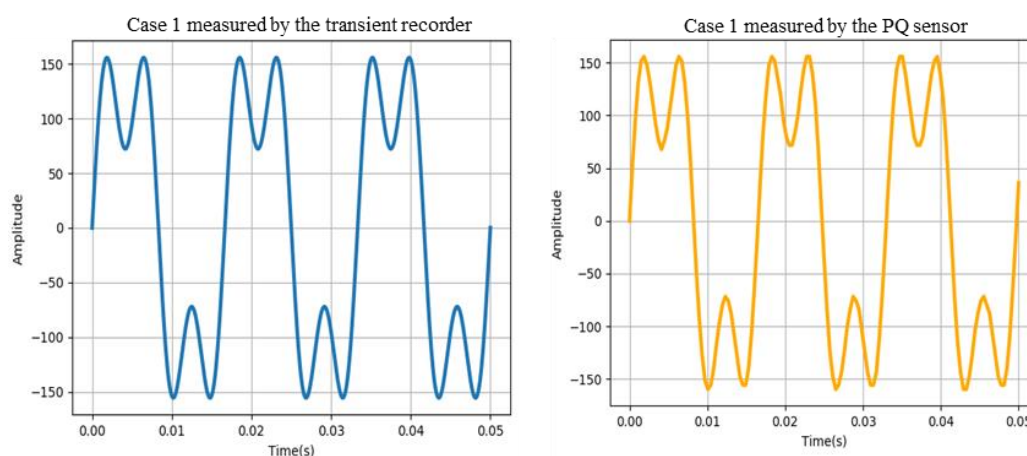


Figure 4-17 Case 1 measured by two devices.

After FFT, it can be seen from Figure 4-18 that there is a significant overlap between the two at 60 Hz and 180 Hz, and the intensity at 60 Hz is about twice that at 180 Hz, so it is consistent with Case 1 set in this study. After the results of the FFT, the statistical

correlation analysis shows that the correlation coefficient between the two is 0.9946 and the RMSE value is 1.9775.

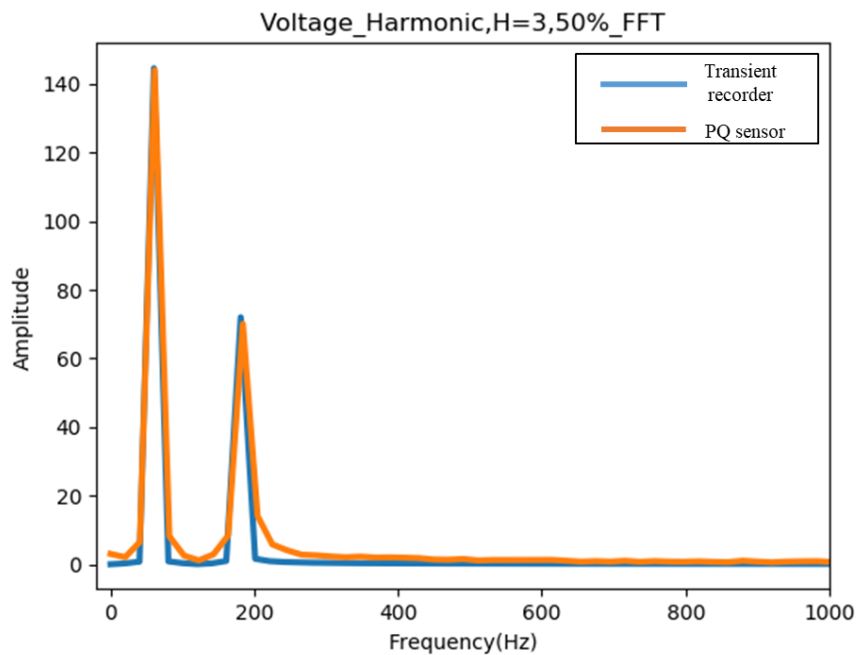


Figure 4-18 Comparison of case 1 after FFT.

In the second case, in order to verify that the system proposed in this study can detect harmonics composed of frequencies of many different levels. Therefore, a harmonic composed of three times (180 Hz) is designed, five times (300 Hz), seven times (420 Hz) and nine times (540 Hz) of the fundamental frequency. Their respective ratios are 2.5 % and the THD is 5 %. The waveform output time lasts 0.05 seconds. The harmonic waveforms of the three cycles as shown in Figure 4-19 are measured by two devices.

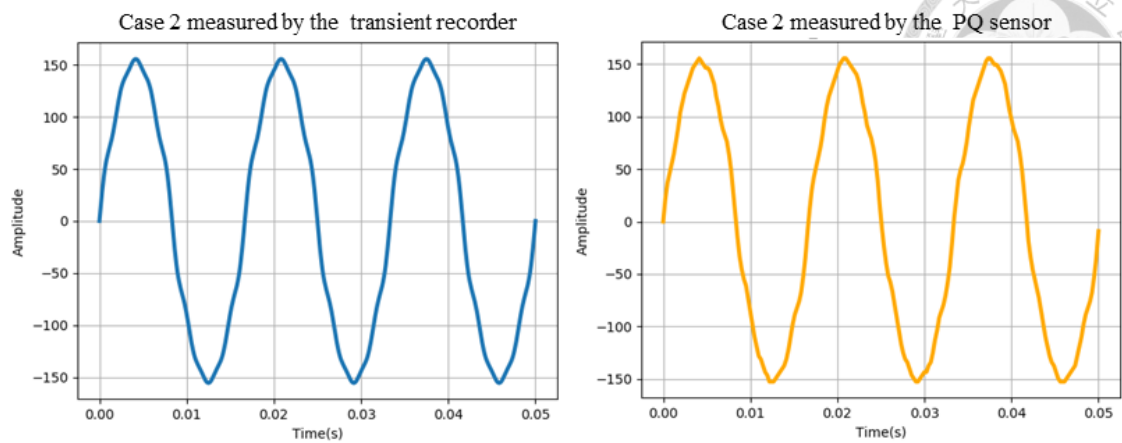


Figure 4-19 Case 2 measured by two devices.

After the FFT, it can be found that the two overlap at the expected five frequencies, and the intensity at 60 Hz is about 40 times that of the other four, so it is consistent with Case 2 set in this study. The correlation coefficient :0.9999 and the RMSE is 0.2740.

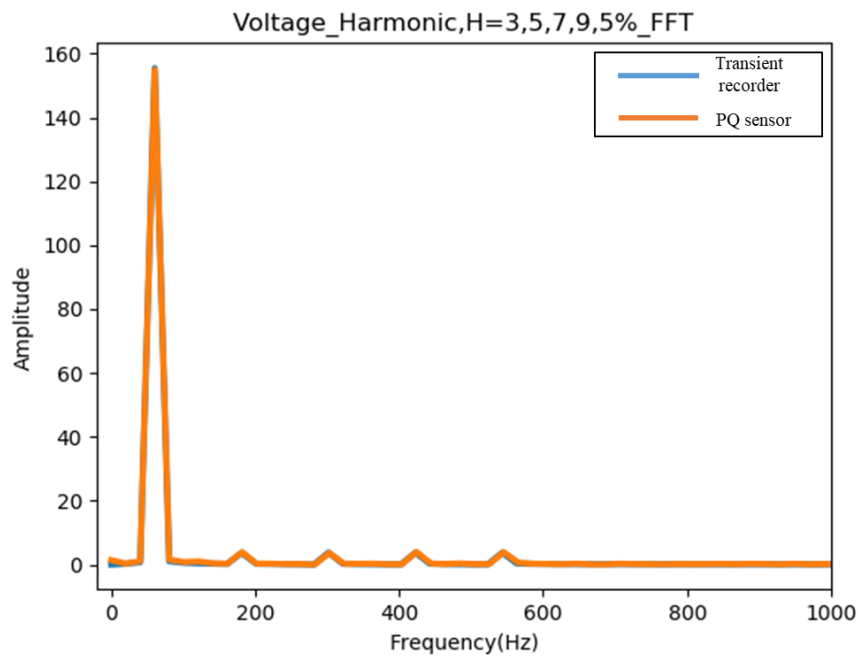


Figure 4-20 Comparison of case 2 after FFT



In the third case of voltage harmonics, in order to verify that the system proposed in this study can detect high-level harmonics, a high-order harmonic containing 3 % of 25 times the fundamental frequency (1500 Hz) is designed. The total duration is 0.05 seconds. The harmonic waveforms of the three cycles as shown in Figure 4-21 are measured by two devices.

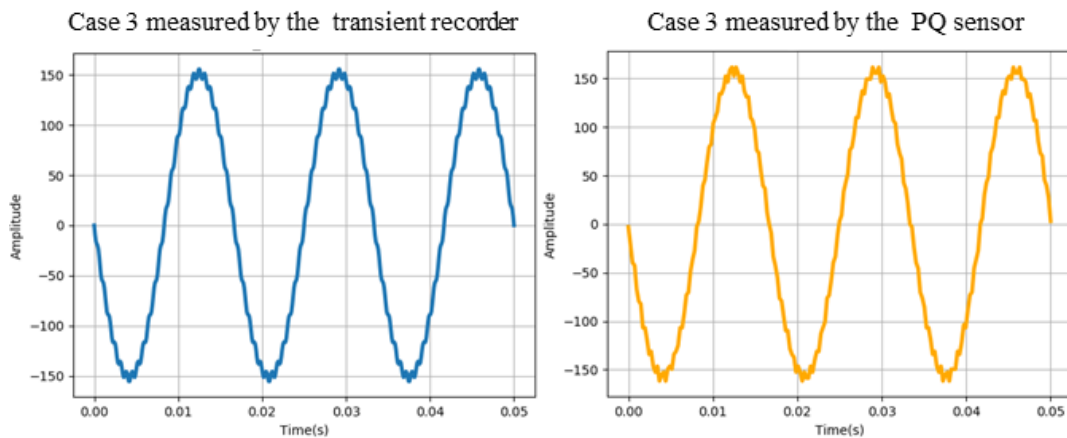


Figure 4-21 Case 3 measured by two devices.

The measurement results after FFT can be found that there is a high overlap between 60Hz and 1500Hz, and the intensity at 60Hz is much higher than 1500 Hz, so it is consistent with Case 3 set in this study. Also, the correlation coefficient is 0.9999 and the RMSE is 0.2107.

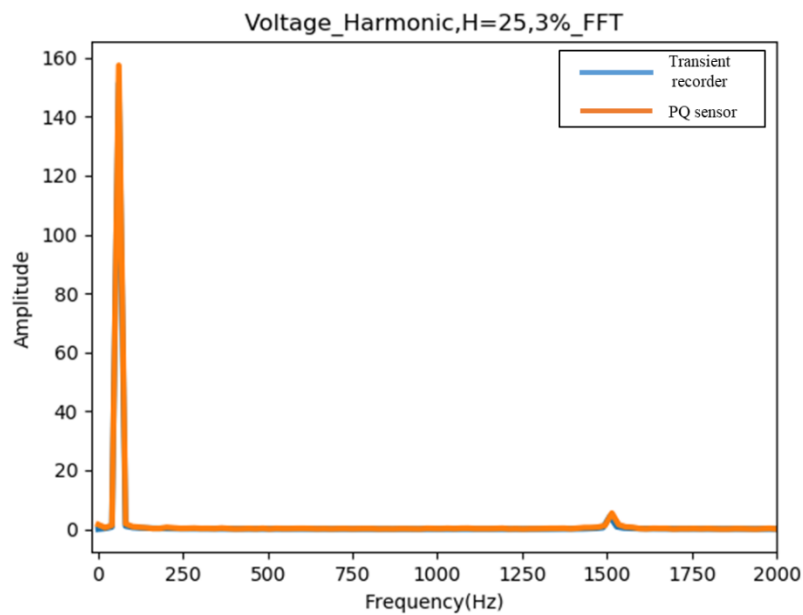


Figure 4-22 Comparison of case 3 after FFT.

In addition to the voltage harmonics mentioned above, current harmonics are also a frequent occurrence of poor power quality. If the sum of harmonic currents exceeds the allowable value, it may cause equipment damage and cause some economic loss. This study sets a set of current harmonics with a current of 25 A, including three times (180 Hz), five times (300 Hz), seven times (420 Hz) and nine times (540 Hz) of the fundamental frequency, and is measured at the output through CT. It lasted for 0.05 seconds, and the current harmonic waveforms of three cycles as shown in Figure 4-23 were measured by two devices.

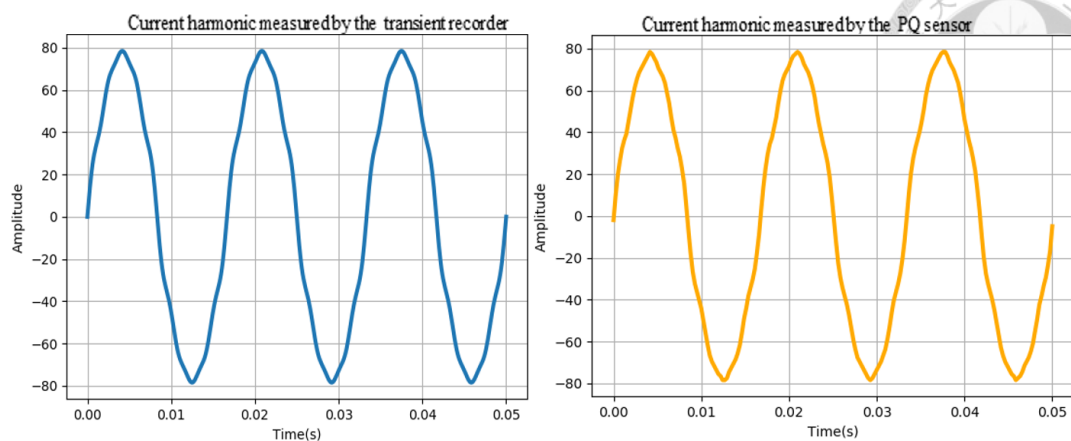


Figure 4-23 Current harmonics measured by two devices.

The current harmonics can be found after the FFT, which is consistent with the results of the voltage harmonic analysis. The two have obvious overlap at the expected five frequencies, and the intensity at 60 Hz is also significantly stronger than the other four. In addition, Also, the correlation coefficient is 0.9993 and the RMSE is 0.5623.

4.3.5 Spectrogram of Poor Power Quality Event

Time-frequency analysis is a generalization of spectrum analysis and is more intuitive than spectrum analysis. When analyzing a signal that changes with time, if only discrete Fourier transform is used, although all the frequency information of the signal can be obtained, the information of time is lacking. The time-frequency analysis multiplies a window function at each sampling time point, and then performs discrete

Fourier transform to know the frequency of the signal during that time. The mathematical expression is as follows.

$$X(t, f) = \int_{-\infty}^{\infty} w(t - \tau)x(\tau)e^{-2j\pi f\tau} d\tau \quad (4-1)$$

It can be seen from the spectrogram of voltage swell event in Figure 4-24, voltage sag event in Figure 4-25 and voltage interruption in Figure 4-26. Although there are some small strengths around the main frequency of 60 Hz, but the highest intensity changes still occurring at 60 Hz.

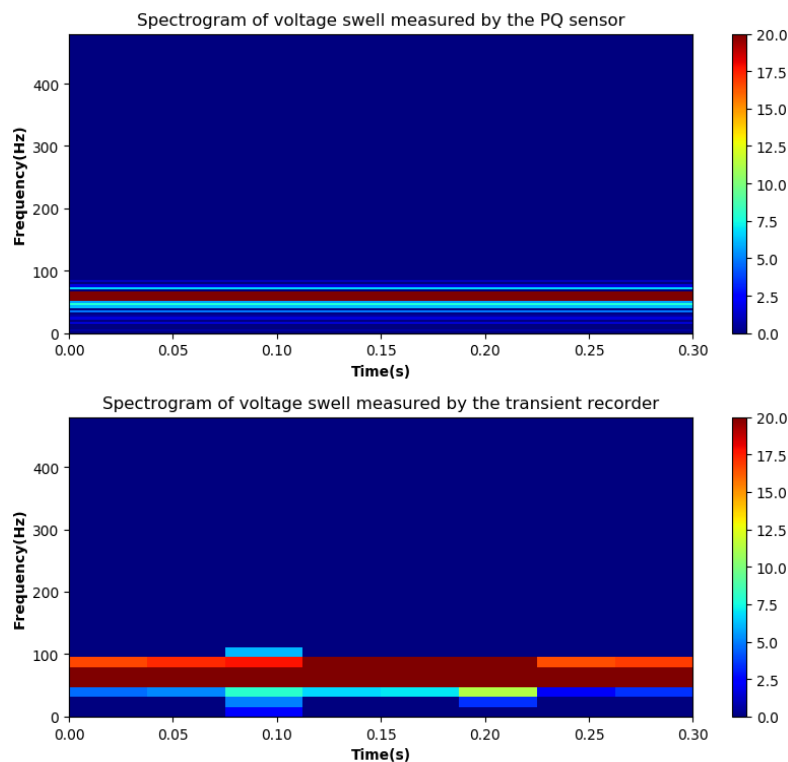


Figure 4-24 The spectrogram of voltage swell event.

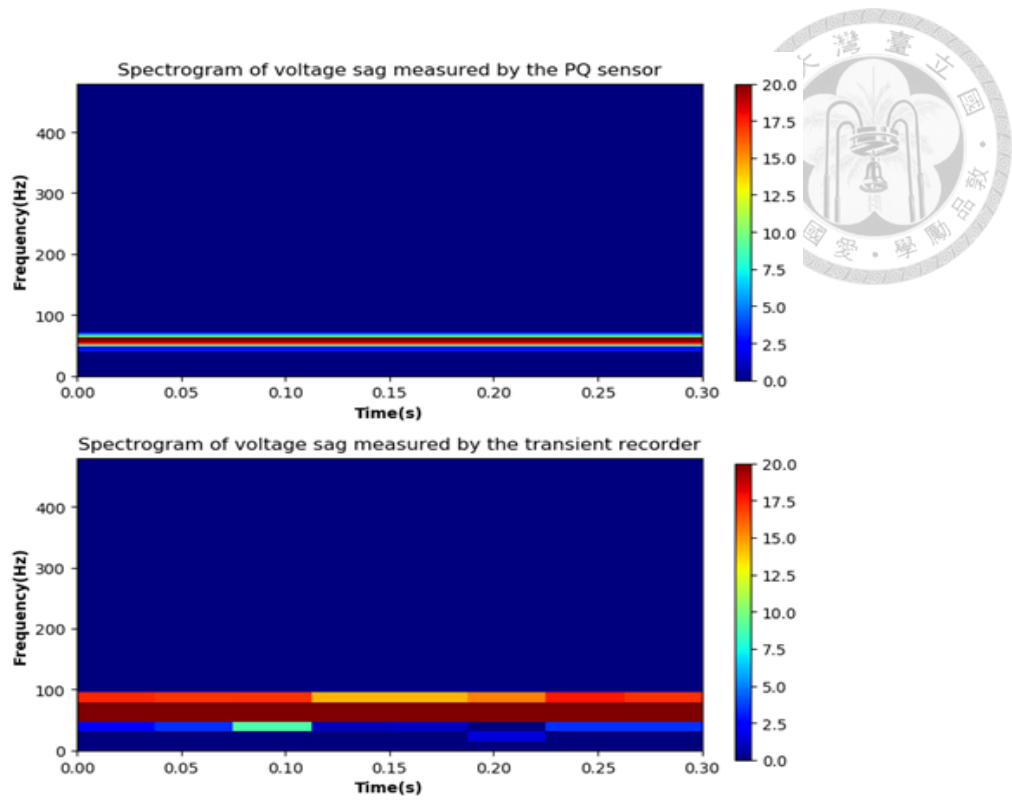


Figure 4-25 The spectrogram of voltage sag event.

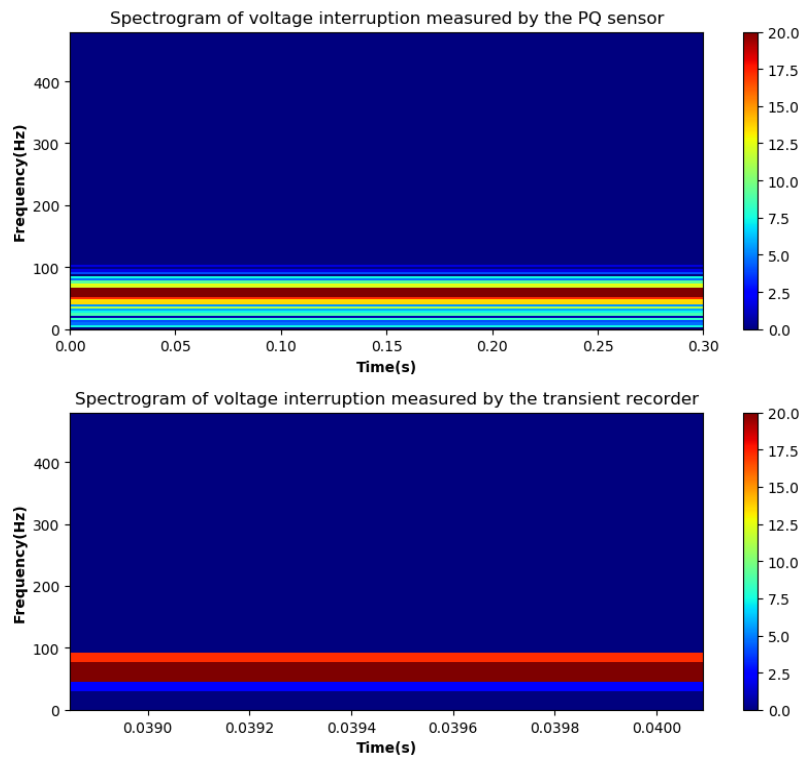


Figure 4-26 The spectrogram of voltage interruption event.

The same, voltage harmonics can also be spectrogram to show the relationship between frequency and time, as can be seen from Figure 4-25. The following three different cases also appear at different intensities at the corresponding frequencies. For example, case 1 has an intensity of 60 dB at 20 Hz and a red color of 14 dB at 180 Hz, which just shows that the intensity at 60 Hz is twice that at 180 Hz. As for case 2, the intensity at 60 Hz is significantly greater than 180 Hz, 300 Hz, 420 Hz and 540 Hz. And case 3 has a large intensity at 60 Hz and 1500 Hz.

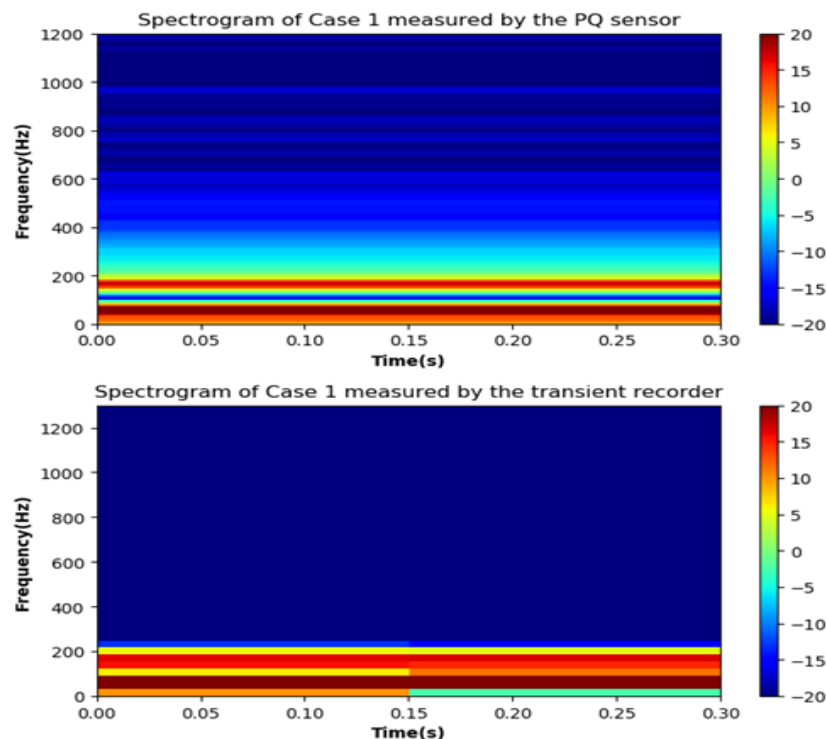


Figure 4-27 The spectrogram of harmonic case 1.

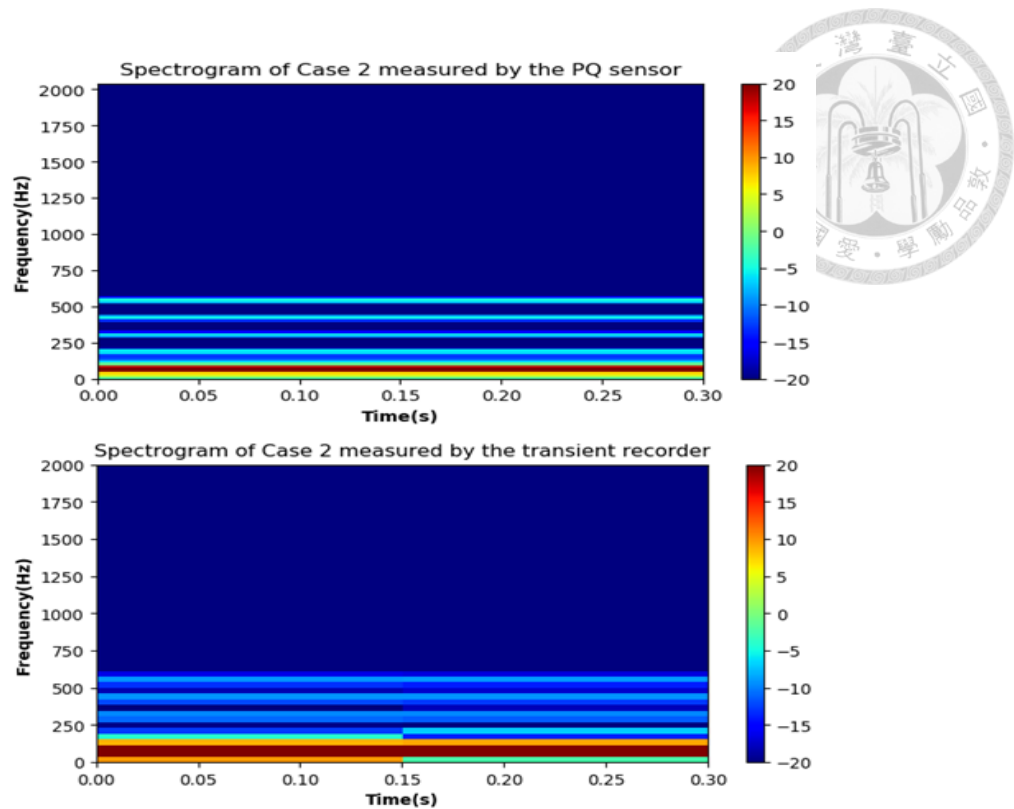


Figure 4-28 The spectrogram of harmonic case 2.

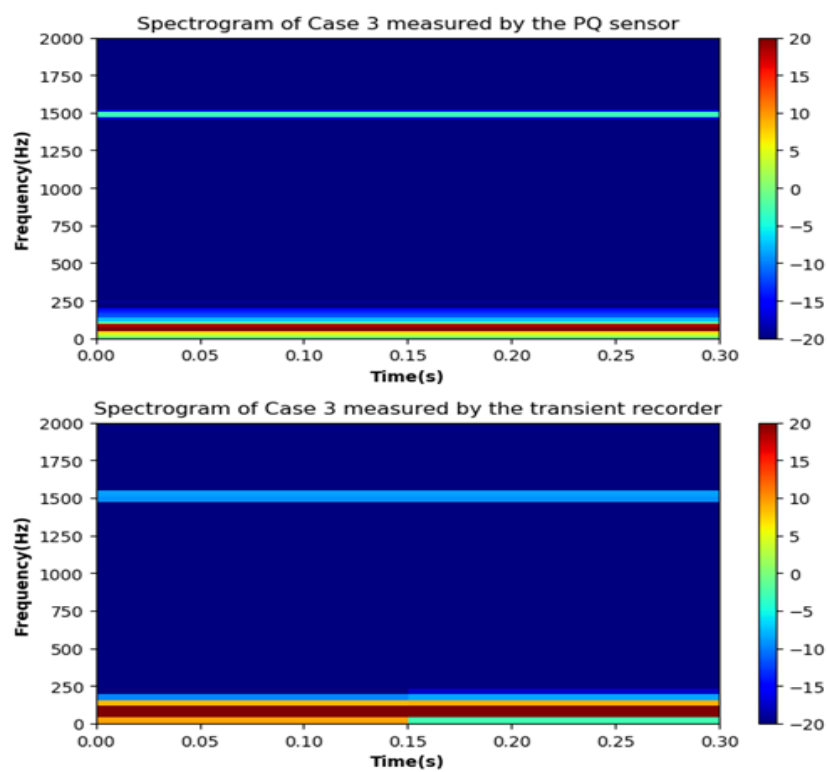


Figure 4-29 The spectrogram of harmonic case 3.



4.4 Field Experiment

In order to verify the IoT architecture of the system, a widely distributed experiment was set up. The location was selected at the Taiwan Power Research Institute, and three CMC356 and three PQ sensors were placed in different rooms (room A, B, C). Then, a gateway device for collecting data is placed in room D, and the distance to the gateway is 20 meters, 25 meters and 20 meters respectively.

4.4.1 Transmission and Receiving Rate of Wireless Transmission

First of all, in order to know whether the data receiving rate and the transmission rate are blocked by large objects (such as heavy iron gates and tall electronic equipment), the transmission rate is still maintained. This study uses the application XCTU, and the Range Test function is being used. if the transmitted packet is not received within 100 ms, it is regarded as a transmission failure. Similarly, if the packet with successful transmission is not received within 100 ms, the reception fails. The experiment tests the transmission rate and receiving rate of one hundred packets within a certain period of time.

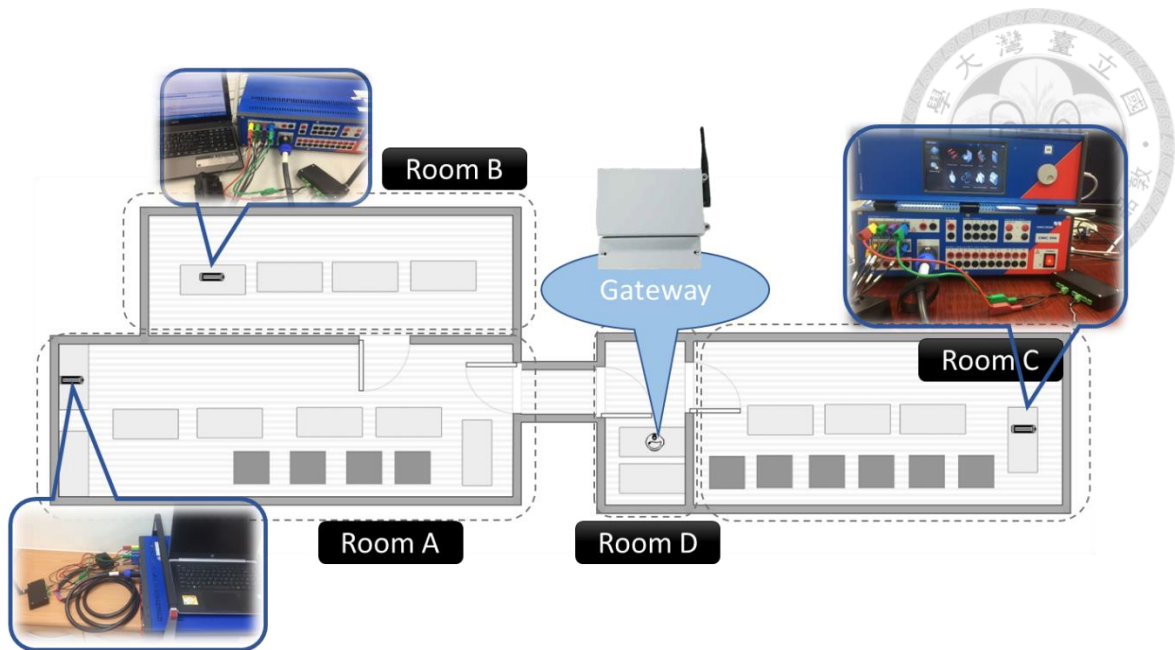


Figure 4-30 System equipment location map.

As can be seen from Figure 4-31, in the test interval, the transmission and reception rates of the three locations are maintained at 100 %, and because the equipment placement point of room A is farther than the other two rooms. Therefore, the average transmission intensity is relatively small and the stability is poor. The average transmission intensity between the equipment located in room C and the gateway is about -70 dBm and the transmission intensity of room B oscillates between -70 dBm and -95 dBm. Although room B has the same transmission distance as room C, however, because room B and the gateway are separated by thick walls and metal doors, the average transmission intensity is weaker than that of room C.

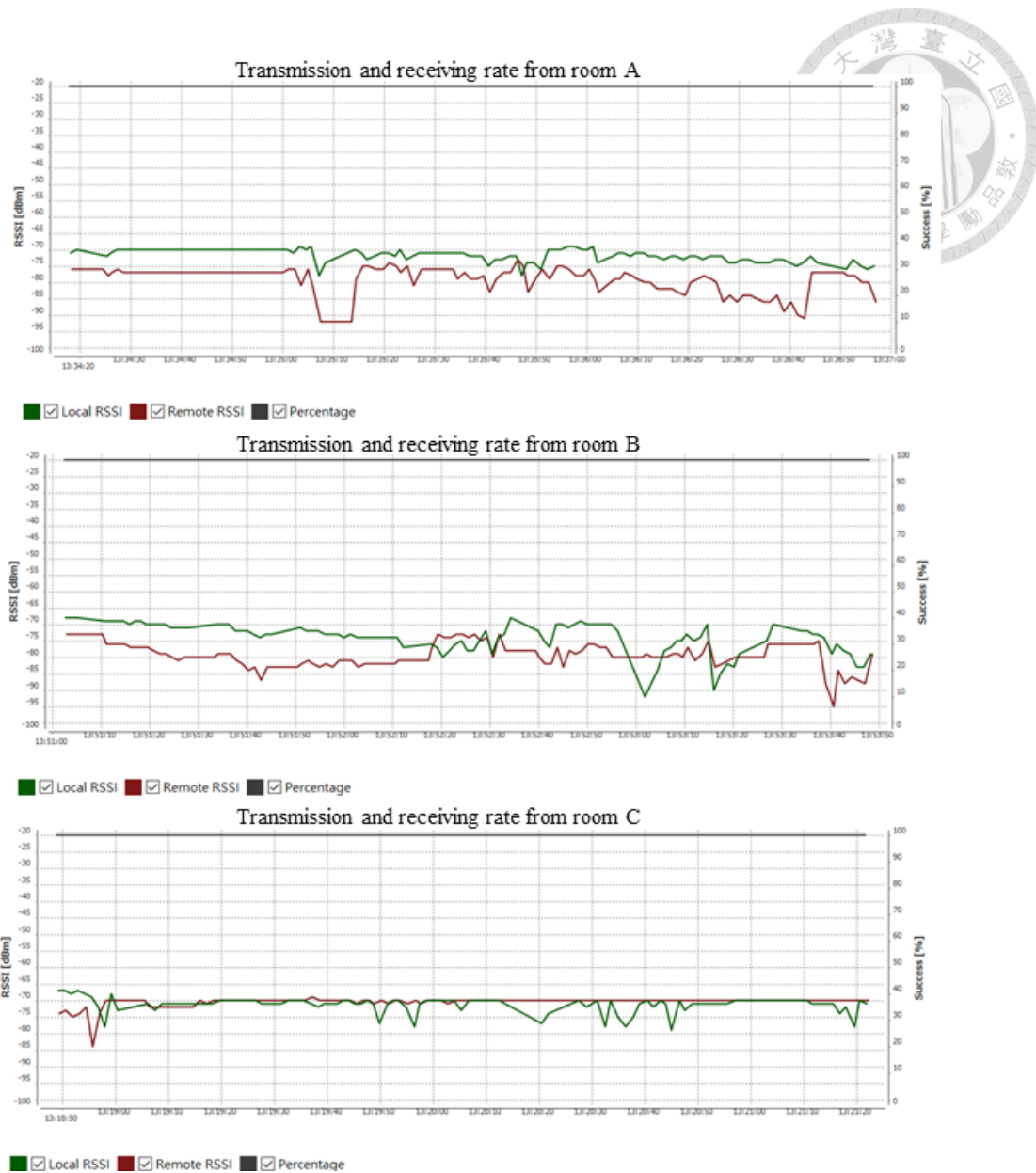


Figure 4-31 Transmission and receiving rate from different room.

4.4.2 Power Quality Event Classification

After proving good and stable transmission and reception capabilities, it is necessary to prove that the system has event recognition capability. When different types of power quality events occur, the types of events can be distinguished to achieve early warning

and record functions. Monitors can take precautions or debug against corresponding problems to facilitate quick restart of system operation.

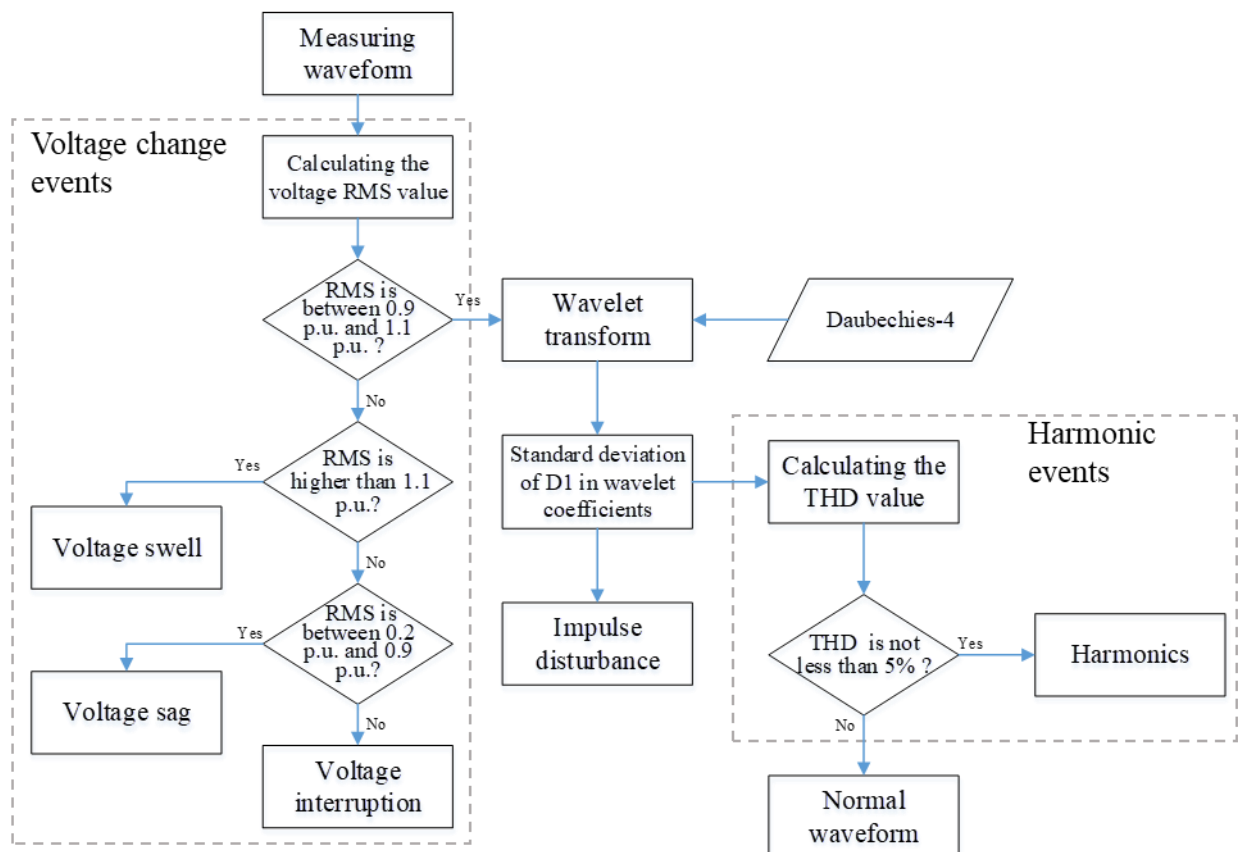


Figure 4-32 Data flow block diagram of the proposed classifier.

This experiment first verifies whether the system's event resolving power is good when a single event occurs. Therefore, three main events as the target of classification. In the voltage swell, voltage sag and voltage interruption based on the voltage RMS, this experiment selects the voltage sag that occurs more frequently and is easy to cause



damage. As one of the experimental objectives, voltage harmonics and current harmonics composed of multiple frequencies were also selected as targets for observation. The X stands for sine wave output.

Table 4-1 Operational script for one power quality events.

Time Room	T_x	T_e	T_x	T_e	T_x	T_e	T_x
A	X	A_1	X	X	X	X	X	A_2	...
B	X	X	X	B_1	X	X	X	X	...
C	X	X	X	X	X	C_1	X	X	...

The event running script is shown in Table 4-1. T_x is the sine wave running time, set to five seconds, and T_e is the event occurrence time, set to 0.3 seconds (18 cycles). This article sets the voltage for normal operation to 110 volts, that the current is 25 amps, and the corresponding event is a voltage sag event with a transient voltage drop of 80 volts. Event 2 contains the fundamental frequency, three times, five times, seven times and nine times. The total Harmonic distortion is 5 % of voltage harmonic events. Event 3

is also a current harmonic event with a fundamental frequency of three, five, seven and nine times and a total harmonic distortion is 5 % of current harmonic events.



Table 4-2 Accuracy of one event classification.

Event Room	A_1	A_2	A_3	B_1	B_2	B_3	C_1	C_2	C_3
A	10	10	10						
B				10	10	10			
C							10	10	10
Receiving rate (%)	100	100	100	100	100	100	100	100	100
Accuracy (%)	100	90	90	100	90	90	100	90	90

This study repeatedly runs the script ten times, and records the total acceptance rate of the ten events and the total classification accuracy rate, as shown in Table 4-2 above. It can be seen from the table that the event receiving rate is consistent with the results of the transmission experiment. Both receiver rates are maintained at 100 %. The accuracy of the voltage sags and voltage harmonic events are above 90 %. In the case of voltage

events, the accuracy of current harmonics is between 80 % and 90 %. This may be because the signal is generated by induction, not directly, so the accuracy in the time domain waveform is worse than the direct amount. The measurement is poor, so the calculation of THD is relatively inaccurate.

Table 4-3 THD of unsuccessful classification events.

	Standard THD value (%)	Sensing THD value (%)
A_2	5	4.91
A_3	5	4.77
B_2	5	4.89
B_3	5	4.72
C_2	5	4.92
C_3	5	4.7

The harmonic threshold set by the original value is 5 %, and the output of the waveform generator is also 5 %. That is, when the THD value is not less than 5 %, the system judges that the harmonic event is generated, and thus the raw data measured by the flow device is calculated. It should also be 5 %. According to the above Table 4-3, the THD calculated without the success of the event is less than 5 %.

After the single event judgment rate is at least 90 % or more, the system also needs to be verified whether the system judgment rate can still be maintained in a good condition when the bad power quality events occur simultaneously. As shown in Table 4-1, this

experiment also sets three bad power quality events. The sine wave is output for five seconds at the T_x time point. Then, at the T_e time point, the two power quality events occur simultaneously. For example, when the first T_e time point, room A and room B have a voltage sag at the same time, and at the second T_e time point, room A and room C simultaneously have a voltage sag. The operation script is shown in Table 4-4. This study repeatedly runs the script ten times, and records the total acceptance rate of the ten events and the total classification accuracy rate, as shown in Table 4-5. As in the above experiment T_x operation time is five seconds, and T_e operation time is 0.3 seconds.

Table 4-4 Operational script for two power quality events.

Time Room	T_x	T_e	T_x	T_e	T_x	T_e	T_x
A	X	A_1	X	A_1	X	A_2	X	A_2	...
B	X	B_1	X	X	X	B_2	X	X	...
C	X	X	X	C_1	X	X	X	C_2	...



Table 4-5 Accuracy of tow event classification.

Event Room	A_1, B_1	A_1, C_1	A_2, B_2	A_2, C_2	A_3, B_3	A_3, C_3	B_1, C_1	B_2, C_2	B_3, C_3
A	10	10	10	10	10	10			
B	10		10		10		10	10	10
C		10		10		10	10	10	10
Receiving rate (%)	100	100	100	100	100	100	100	100	100
Accuracy (%)	90	90	90	90	90	90	90	90	90

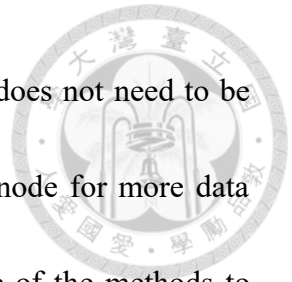
As can be seen from Table 4-5, the receiving rate is maintained at 100 % as in the above two experiments, and the event judgment rate also 90 %, while event three is obviously clearly the same as the other two. Compared with single event detection, obviously, the accuracy rate of event one and event two is slightly decreased. The possible reason is that judging two events at the same time will cause the system operation amount to increase slightly, resulting in a decrease in accuracy.

Chapter 5 Conclusions and Future work



This study proposes a low-cost wireless power quality monitoring system. It proves the accuracy and reliability of the measurement results by comparing with the measurement results of the commercially available transient recording instruments. Moreover, the findings presented in section 4.2.2 demonstrate the feasibility of a large scale deployment of the IoT-based power quality monitoring system to improve the safety of power grids. The wireless monitoring system proposed in this study is aimed at different power quality events, such as instantaneous voltage changes, voltage harmonics and current harmonics. It can be seen from the experiment in Chapter 4. Comparing the measured results of the system with the results measured by commercially available instruments, a high correlation coefficient and a low RMSE value can be obtained. Also, the accuracy of the classification results is at least 90 %. The above indicates the reliability of the system. According to the sampling theorem, the higher the sampling frequency, the more accurate the measurement result can be obtained. Although the high accuracy can be obtained at this sampling frequency, the higher sampling frequency is better based on hardware optimization. So far, the system only measures voltage transients and harmonic distortions, and only uses waveform generators for experiments. Therefore, the sampling rate needs to be improved, and more power quality events can be measured and the actual


field test must be further research in the future. If the sensing data does not need to be transmitted through the gateway, it can directly sit on the sensing node for more data analysis, event classification and data uploading, which is also one of the methods to simplify the system. Through this power quality monitoring system, the management of power equipment and the safety of the power grid are greatly improved, and in the event of an accident, it can be known that the supplier or the user needs to be responsible. And it is one of the best solutions for achieving smart grid goals.

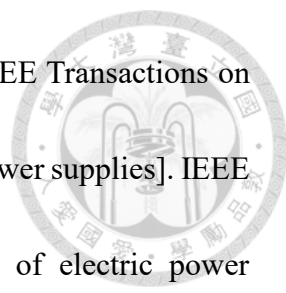


References



- 江榮城。2007。電力品質，臺北：全華圖書出版社。
- 呂榮基，江瑞利，黃厚生，蘇俊連，殷世安譯。2005。電力系統品質。臺北：美商麥格羅·希爾國際股份有限公司。
- Begovic, M. M., Djuric, P. M., Dunlap, S., and Phadke, A. G. 1993. Frequency tracking in power networks in the presence of harmonics. *IEEE Transactions on Power Delivery*, 8(2): 480-486.
- Bollen, M. H. 2000. Understanding power quality problems. In "Voltage sags and Interruptions". New York: IEEE press.
- Bonner, A., Grebe, T., Gunther, E., Hopkins, L., Mahseredjian, J., Miller, N., Ortmeier, T., Rajagopalan, V., Ranade, S., and Ribeiro, P. 1996. Modeling and simulation of the propagation of harmonics in electric power networks. 2. sample systems and examples. *IEEE Transactions on Power Delivery*, 11(1): 466-474.
- Brito, N., Souza, B., and Pires, F. 1998. Daubechies wavelets in quality of electrical power. 8th International Conference on Harmonics and Quality of Power. Proceedings (Cat. No. 98EX227), Athens, Greece.
- Chen, Y. C., and Lan, J. K. 2014. Implementation of power measurement system with Fourier series and zero-crossing algorithm. 2014 International Symposium on Computer, Consumer and Control, Taichung, Taiwan.
- Cooley, J. W., and Tukey, J. W. 1965. An algorithm for the machine calculation of complex Fourier series. *Mathematics of computation*, 19(90): 297-301.
- Cristaldi, L., and Ferrero, A. 1995. A method and related digital instrument for the measurement of the electric power quality. *IEEE Transactions on Power Delivery*, 10(3): 1183-1189.
- Dash, P., Panigrahi, B., and Panda, G. 2003. Power quality analysis using S-transform. *IEEE Transactions on Power Delivery*, 18(2): 406-411.
- Daubechies, I. 1990. The wavelet transform, time-frequency localization and signal analysis. *IEEE transactions on information theory*, 36(5): 961-1005.
- Douglas, J. 1993. Solving problems of power quality. *EPRI journal*, 18(8): 6-16.
- Gray, W., and Haydock, F. 1995. Industrial power quality considerations when installing adjustable speed drive systems. 1995 IEEE Cement Industry Technical Conference. 37th Conference Record, San Juan, Puerto Rico, USA.

- 
- Huang, Z., Zhu, T., Lu, H., and Gao, W. 2016. Accurate power quality monitoring in microgrids. 2016 15th ACM/IEEE International Conference on Information Processing in Sensor Networks (IPSN), Vienna, Austria.
- IEEE Std 519-1992. 1993. IEEE Recommended Practices and Requirements for Harmonic Control in Electrical Power Systems.
- IEEE Std 1159-2009 2009. IEEE Recommended Practice for Monitoring Electric Power Quality.
- Jurado, F., and Saenz, J. R. 2002. Comparison between discrete STFT and wavelets for the analysis of power quality events. *Electric Power Systems Research*, 62(3): 183-190.
- Kazibwe, W. E., Ringlee, R. J., Woodzell, G. W., and Sendaula, H. M. 1990. Power quality: a review. *IEEE Computer Applications in power*, 3(1): 39-42.
- Koval, D. O., and Carter, C. 1997. Power quality characteristics of computer loads. *IEEE Transactions on Industry Applications*, 33(3): 613-621.
- Lang, M., Guo, H., Odegard, J. E., Burrus, C. S., and Wells, R. O. 1996. Noise reduction using an undecimated discrete wavelet transform. *IEEE Signal Processing Letters*, 3(1): 10-12.
- Lee, J.-S., Su, Y.-W., and Shen, C.-C. 2007. A comparative study of wireless protocols: Bluetooth, UWB, ZigBee, and Wi-Fi. *Industrial electronics society*, 5: 46-51.
- Lentz, R. C., Mercede, F. J., and Mercede, J. 1995. A student design project to improve power quality for a commercial facility. *IEEE transactions on power systems*, 10(1): 3-10.
- Mog, G. E., and Ribeiro, E. P. 2004. Zero crossing determination by linear interpolation of sampled sinusoidal signals. 2004 IEEE/PES Transmission and Distribution Conference and Exposition: Latin America (IEEE Cat. No. 04EX956), Sao Paulo, Brazil.
- Morales-Velazquez, L., de Jesus Romero-Troncoso, R., Herrera-Ruiz, G., Morinigo-Sotelo, D., and Osornio-Rios, R. A. 2017. Smart sensor network for power quality monitoring in electrical installations. *Measurement*, 103: 133-142.
- Naidoo, R., and Pillay, P. 2007. A new method of voltage sag and swell detection. *IEEE Transactions on Power Delivery*, 22(2): 1056-1063.
- Narcowich, F. J., and Boggess, A. 2009. A first course in wavelets with Fourier analysis: Wiley.
- Proakis, J. G., and Manolakis, D. G. 1995. *Digital Signal Processing: Principles, Algorithms, and Edition*: Prentice Hall, Upper Saddle River, New Jersey.

- 
- Reid, W. E. 1996. Power quality issues-standards and guidelines. IEEE Transactions on Industry Applications, 32(3): 625-632.
- Sabin, D. D., and Sundaram, A. 1996. Quality enhances reliability [power supplies]. IEEE spectrum, 33(2): 34-41.
- Song, Y., Yuan, F., Chenlong, G., and Naibao, H. 2011. Design of electric power parameter monitoring system based on dsp and cpld. 2011 Fourth International Conference on Intelligent Computation Technology and Automation, Shenzhen, Guangdong, China.
- Zhang, M., and Li, K. 2009. A power quality monitoring system over the internet. 2009 First International Conference on Information Science and Engineering, Nanjing, China.